Importance of Asphalt Binder Properties on Rut Resistance of Asphalt Mixture

by

Amir Arshadi

A thesis submitted in partial fulfillment of
the requirements for the degree of

Master of Science
(CIVIL & ENVIRONMENTAL ENGINEERING)

at the

UNIVERSITY OF WISCONSIN-MADISON

2013

ABSTRACT

Permanent deformation in asphalt mixture, also known as “rutting”, is one of the most important distresses observed in asphalt pavements. Rutting in the asphalt mixture layer is the permanent deformation of the asphaltic layer near the surface. As the binder phase is responsible for the viscoelastic behavior of a mixture, it plays a dominant part in determining many of the aspects of pavement performance, such as resistance to permanent deformation. This phenomenon is more critical during the warm season of the earlier period of pavement life due to the asphalt binder lower stiffness.

To strengthen asphalt pavements against damage, modifiers are added to the asphalt binder. The polymers that are used for binder modification can be divided into two broad categories, namely plastomers and elastomers. Plastomers increase the binder’s stiffness and toughness, while elastomers are known to increase the stiffness and elastic response.

Elastic and viscous response of binders are important aspects in the behavior of polymer modified binders and are believed to have an important role in rut resistance of asphalt mixture, although the exact nature of their effect is not well understood. In this study, finite element simulation and image analysis were used to simulate the behavior of asphalt mixture and study the effect of elastic and viscous component of binder behavior on performance of asphalt mixture in rutting. Finite element method provides data that cannot be directly obtained from experiments and are not readily accessible, such as information regarding local stress and strain distribution of the components in the aggregate structure. A multi-scale approach was developed and used to investigate the performance of asphalt mixture across a number of scales. Binder viscoelastic properties used in the analysis were derived from analysis of rheological data derived using a Dynamic Shear Rheometer (DSR), and were consequently used to determine the viscoelastic

properties of the mastic scale. Mastic scale response was used in the mortar scale. Finally the mortar scale response provided the input to the asphalt mixture scale. The results of this dissertation prove the hypothesis that binder elastic properties and viscous properties affect the rut resistance of hot mix asphalt. It is shown that the permanent deformation of the mixtures containing binders with higher viscous component (lower permanent deformation) is lower. It is also concluded that for the binders with same permanent deformation under the same step stress (same viscous component), higher elastic response of binder leads to lower permanent deformation of the asphalt mixture; however the effect of elastic component on rutting is minor in comparison with the effect of asphalt binder viscous component.

In the case of aggregate gradation it is shown that a well-graded, intermediate gradation is capable of generating effective particle networks in micro- and macro-scale, thus reducing binder stress levels over all scales of the asphalt mixture. Overly fine aggregate gradation could prevent effective formation of aggregate skeletons at the macro scale. On the other hand use of overly coarse gradations leads to lower volume fractions of fine particles, impeding network formations and leading to softer mastic and mortar matrixes.

It is shown that the structure of asphalt mixture changes continuously during the repeated creep loading test. It is believed that at the end of the secondary zone of rutting large deformations are initiated in the asphalt mixture resulting in degradation of the structure of the aggregates. This stage is the beginning of the tertiary zone of rutting.

This study focuses on the effect of binder response elastic component and viscous component on rutting resistance of asphalt mixtures in primary and secondary zones where the structure of the mixture has not been degraded significantly due to initiation of large deformations. The results of this study clearly demonstrates, that mixtures containing binders with higher viscous component show lower permanent deformation. In such a context, the effect of viscous properties of the binder on rutting resistance of asphalt mixture is significantly higher than its elastic response.

TABLE OF CONTENTS

Contents

LIST OF FIGURES

LIST OF TABLES

ACKNOWLEDGEMENTS

I would like to express my regards to my advisor, Professor Bahia, for all of the supports, encouragements, and counseling he provided during my master program.

A sincere thank you is offered to Dr. Hassan Tabatabaee for his lasting and precious assistance through this research.

I would also like to extend my gratitude to the members of my graduate committee: Dr. Likos, and Dr. Parra-Montesinos for their help.

The greatest appreciation to everyone from the Asphalt Research Group of the University of Wisconsin-Madison, especially my dearest friends, Dr. Raul Velasquez, and Nima Roohi.

To Mom, Dad, and Elika

1. Introduction

1.1 Background

One of the most important distresses in the asphalt mixture, particularly in the warm seasons, is the permanent deformation of the pavement layers under repeated traffic load, or “rutting”. Rutting can occur in the subgrade, base or asphaltic layers depending on the magnitude of the traffic load and the relative stiffness of the pavement layers. Rutting in the asphalt layer is the result of structural deficiencies in the aggregate or binder phase.

Two mechanisms are commonly associated with rutting in the asphalt layer: vertical consolidation and lateral distortion. As the aggregate and binder phases are nearly known to be incompressible; most of the volume loss in HMA mixtures is thought to be due to the reduction in volume of air voids. Theoretical and laboratory studies [1, 2, 3] have shown that shape distortion (shear), which is usually a result of mixture design problem, is the main contributor in rutting, compared to volume change. The rate of both of these types of rutting can increase if too low air void content is [4]. Beer et al. showed that the development of permanent deformation in asphaltic layer of hot mixt asphalt (HMA) is directly related to the stress distribution in the binder phase of the asphalt mixture [5].

To strengthen asphalt pavements against damage, modifiers are sometimes added to the asphalt binder to improve one or more of its basic properties [6, 7, 8]. These properties include viscosity, elasticity, brittleness, storage stability and durability and resistance to accumulated damage. The polymers that are used for binder modification can be divided into two broad categories, namely plastomers and elastomers. Plastomers make the binder’s network more rigid and tough while elastomers make binder’s response highly elastic [9].

Rheological behavior of modifiers containing elastomers and plastomers are widely different especially in viscosity and elastic recovery [10, 11]. As the relative importance and role of binder elasticity is not well understood, there is an essential need to study the effect of binder elasticity in the rut resistance of asphalt mixture.

1.2 Problem Statement

There are two common experiments used to study the behavior of asphalt mixtures in rutting: through binder testing, using the Superpave G*/sinδ parameter and Multiple Stress Creep and Recovery test (MSCR), and through mixture testing under repeated or static loading using the flow time or flow number procedures. Although these tests can help rank materials in terms of total permanent deformation and bulk recovery of the material after unloading, they are limited in their ability to determine the sources of variation of rutting resistance; whether it be a certain binder property (i.e. viscosity and elasticity), aggregate structure, or and combined interaction of both parameters. Such limitation have led to uncertainty in selection of optimum binder and modifier characteristics for maximizing rutting resistance, especially in terms of elastic component and viscous component, two discriminating factors between elastomeric and plastomeric polymer modifiers.

Finite element simulation and image analysis are recent methods used to study the behavior of asphalt mixtures. These methods provide information that cannot be directly obtained from experimental data, such as local stress and strain distribution in asphalt mixture components and the evolution of mixture microstructure and micromechanical response under loading. It is believed that a study combining experimentally measured response from binder and mixture rut resistance tests in combination with image analysis and micromechanical multi-scale

analysis of the asphalt mixture can shed light on the aforementioned questions, leading to a better understanding of the effect of asphalt binder properties on mixture response and performance and forming a basis for better selection of suitable modification techniques for enhancing rutting resistance of asphalt pavements.

1.3 Hypothesis

It is hypothesized that the binder elasticity and binder viscosity affect the stress distribution and permanent strain in binder phase; consequently effecting rut resistance of asphalt mixture.

1.4 Objectives

The objectives of this research are to:

- Define binder response mechanism to strain and permanent deformation in the mixture.
- Study the stress and strain distribution in binder phase in terms of binder elasticity, binder viscosity, and aggregate gradation.
- Providing recommendation with regard to optimum binder modification type to increase rut resistance.

1.5 Outline

This study is separated into nine chapters:

- *Chapter 1: Introduction*

  The introduction includes background information on modification of asphalt binder, a problem statement, hypothesis, and objectives of this research.

- *Chapter 2: Literature Review*

This chapter is divided into seven separate sections: binder modification, rutting in asphalt mixture, characterization of asphalt rutting performance, image analysis, finite element analysis, multi-scaling, and main conclusions.

- *Chapter 3: Methods and Material (Finite Element Modeling, Multi-scale Modeling, Validating Multi-scale Model)*

  In this chapter the multi-scale model is developed and validated with experimental data.

- *Chapter 4: Tracking Micro-structure Changes of HMA during Rutting*

  In this chapter the changing of aggregate structure in different zones of rutting is studied.

- *Chapter 5: Stress and Strain Distribution in Mixture under loading*

  The effect of binder elasticity and binder stiffness on stress and strain distribution of asphalt binder is studied in this chapter.

- *Chapter 6: Practical Application*

  The focus of this chapter is on practical application of this study.

- *Chapter 7: Conclusions*

  The findings gathered from the most relevant analysis of results are summarized in this section.

- *Chapter 8: Recommendations for Future Work*

  Directions for future work are provided in this section.

2. Literature Review

2.1 Binder Modification

Asphalt binder is a product of crude petroleum refining, used for road paving, roofing, adhesives, coatings and construction. Asphalt binder is the only fraction of crude petroleum which does not volatilize during the distillation process. Having a material which satisfies standard specifications for paving is the final goal in production of asphalt binder from crude petroleum refining. It has been shown that adding modifiers to asphalt binder improves its properties to meet standard specifications for road paving. Using modifiers in the production of asphalt pavements has been carried out since the 1970s [11]. Modifiers have been used in the asphalt binder to improve pavement resistance to rutting, thermal cracking, fatigue, stripping and oxidation [12].

An ideal binder in terms of performance has a low temperature susceptibility and enhanced cohesion in all service temperatures [13]. Polymer modification has been increased in the last years. Researchers have shown that using polymers can improve asphalt binder resistance at high and low temperatures. In other words polymer modified asphalt binders can improve overall performance of the pavement [6, 12, 14].

The polymers that are used for binder modification in North America can be divided into two broad categories, namely plastomers and elastomers. The former make the binder's network more rigid and tough while the latter make binder's response highly elastic [9]. Isacsson and Lu (2000) showed that elastomer and plastomer modified binders have widely different rheological properties especially at high temperatures [10].

Styrene butadiene styrene (SBS) is an example of elastomers, the most common polymer used in modification of asphalt binders. Polybutadiene (PBD), Styrene-butadiene rubber latex

(SBR) and crumb rubber (CR) are other common elastomers. The most common plastomers used in asphalt binders are Ethylene vinyl acetate (EVA) and Poly Ethylene (PE) which make the polymer modified asphalt (PMA) stiffer than the base. The resultant binder performance grades using EVA are dependent on the vinyl acetate content and their molecular weight [13].

A modified binder consists of two distinct phases: binder and additive. Brule (2007) showed that by changing the polymer content of PMBs, three different cases can be achieved [13]:

- Low polymer content (less than 4 percent): in this case the polymer phase is dispersed through the binder phase which is the continuous matrix of the PMB (Figure 2-1). At high temperatures the polymer has higher stiffness than the matrix, which increases the mechanical performance of the binder. At low temperatures the polymer's stiffness is less than binder's, which reduces its brittleness. It should be noted that in this case the binder is the determining factor.

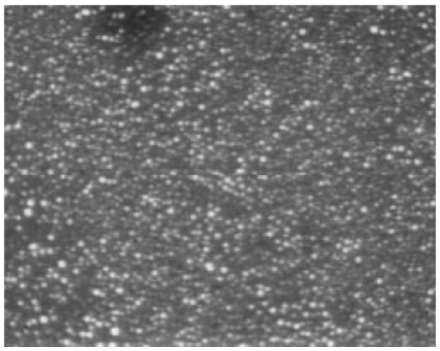

Figure 2-1: Microstructure of a modified binder with binder matrix [13]

- High polymer content (more than 7 percent): in this case the polymer is the matrix of the system (Figure 2-2). The properties of such a system are essentially dependent on the polymer, not the binder.

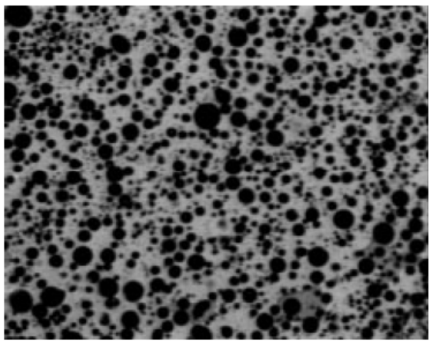

Figure 2-2: Microstructure of a modified binder with polymer matrix [13]

- Around 5 percent polymer content: in this case both of the binder and polymer phases are continuous in the system (Figure 2-3).

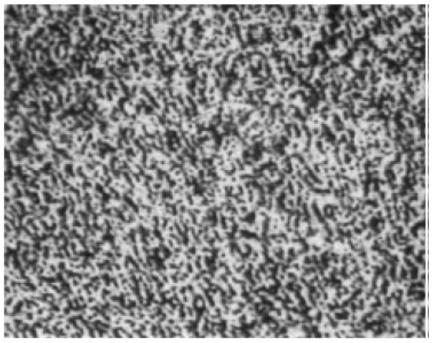

Figure 2-3: Microstructure of a modified binder with two continuous phases [13]

Physical properties of the PMBs are directly dependent on their micro-texture. In another word the properties of a modified binder is related to the chemical reaction of polymer and the binder and how much the polymer swells by absorbing the oily fractions of the binder.

During the National Cooperative Highway Research Program (NCHRP) project 9-10 [6], researchers performed a comprehensive study of the effect of asphalt binder modification on performance of HMA. In terms of rutting it was determined that at a given binder superpave performance grade ,as determined following AASHTO M320, in case of angular aggregates, the effect of binder modification is comparable with effect of aggregate gradation. It was also concluded that the performance grading system cannot offer a reasonable criterion for ranking

the rutting behavior of asphalt mixtures with the same aggregate gradation. Researchers also showed that modification of asphalt binder can significantly affect the fatigue performance, low temperature behavior and rheological behavior of asphalt mixtures. Furthermore in a recent research, Roohi et al. (2012) showed that binder modification can affect the internal structure of asphalt mixture depending on the binder modification type [15].

2.2 Rutting in Asphalt Mixture

Rutting is the accumulation of permanent deformation under load applications in asphalt concrete pavements. Heavy truck traffic and using of high pressure tires have made the problem of rutting more severe. The quality of the materials used in asphalt pavements has an important role in rutting susceptibility of the pavement.

There are many factors which affect the rutting performance of asphalt mixtures. According to the literature the most important factors are: (1) aggregate surface texture, (2) aggregate gradation, (3) aggregate shape, (4) aggregate size, (5) binder stiffness, (6) binder content, (7) air void content, (8) Voids in the Mineral Aggregate (VMA), (9) method of compaction, (10) temperature, and (11) load repetitions.

Rutting is resulted by combination of vertical consolidation and shear deformation in asphaltic layers and also permanent deformation in base, sub-base and subgrade layers. As the asphaltic layers are directly in contact with wheels, they are subjected to very high stresses in comparison with lower layers. Therefore often the rutting of the asphalt pavements is due to permanent deformation of asphaltic layers. Hofstra and Klomp (1972) indicated that shear deformation is the primary rutting mechanism in the asphalt mixtures [16].

A research work of Eisenmann and Hilmer (1987) also showed that the rutting in asphalt mixtures is mainly caused by shear deformation without volume change [17]. As it can be seen in (Figure 2-4), during the initial stage of wheel passes the increase of irreversible deformation beneath the tires is much greater than the increase in upheaval zones. It shows that at the initial stage of wheel passes, most of the permanent deformation is due to consolidation of the asphalt mixture. Figure 2-4 shows that after initial stage, the decrement of volume beneath the tires is almost the same as increment of volume in the upheaval zones.

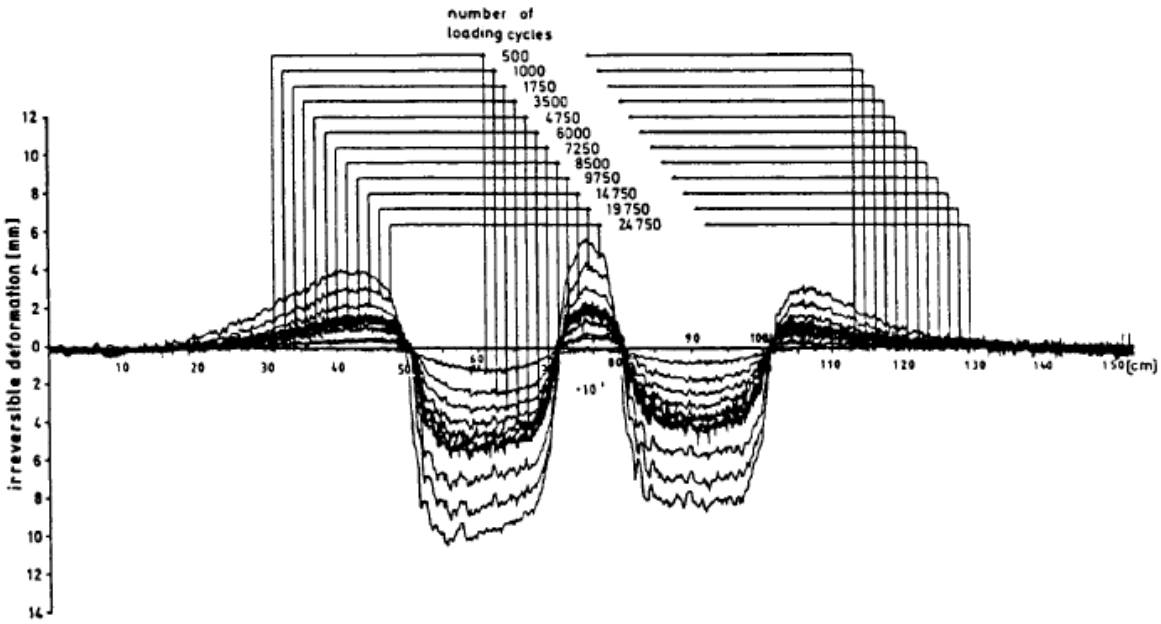

Figure 2-4: Effect of number of passes on transverse surface profile [17]

Uge and Van de Lu (1974) indicated that the rutting resistance of asphalt mixture is dependent on its thickness [18]. They showed that by increasing the asphalt layer thickness its rutting performance increases, up to a threshold thickness (13 cm) after which the rut resistance of asphalt mixture does not change significantly.

Mahboub and Little (1988) showed that the low viscosity binders make the asphalt pavements more rutting susceptible [19]. In another research, Monismith et al. (1985)

recommended using of harder (more viscous) binders in thicker asphalt layers and hotter climates [20]. As it was mentioned earlier, modifiers are used to increase the asphalt binder viscosity at higher temperatures without deteriorating its properties at lower temperatures.

Brown and Bell (1977) concluded that gap graded mixtures are more rutting susceptible than the well graded mixtures due to the lower number of aggregate contact points and consequently less aggregate interlock [21]. They further argued that at the higher temperatures, as the aggregate interlock becomes more dominant in rutting performance of asphalt mixtures, gap graded mixtures may show significantly higher rutting susceptibility than the well graded mixtures. Davis (1988) reported that some asphalt mixtures constructed with large maximum aggregate size (1½ in. or larger) exhibit low rutting susceptibility [22]. Based on those observations it was concluded that using of larger maximum aggregate size (about two-thirds of layer thickness) would increase the rutting resistance of asphalt mixtures subjected to high pressure.

The aggregate surface texture and particle shape play important roles in rutting resistance of asphalt mixtures especially in thicker asphalt bound layers and hot climates. Mixtures made from angular aggregates are more rut resistant and stable than the mixtures with the same gradation and composition but using rounded aggregates. It should be noted that the aggregate surface texture and shape are interrelated [18].

2.3 Characterization of Asphalt Rutting Performance

The main goal of material testing is to simulate the pavement situ conditions in the laboratory as similar as possible. There are different conditions that should be considered, including stress state, temperature, moisture, and general condition of the material. Based on SHRP (1991) there

are four different types of tests used to characterize the rutting response of the asphalt pavements, including: (1) uniaxial stress tests: “Unconfined testing of cylindrical samples in creep, repeated creep or dynamic loading”, (2) tri-axial stress tests: “Confined testing of cylindrical samples in creep, repeated creep or dynamic loading”, (3) diametral loading tests: “Briquette specimens in creep or repeated loading”, and (4) wheel-track tests: “Testing the slab of prepared or actual pavement using a repeated passing wheel”.

Many researchers have shown that the tri-axial test represents the material stress state in the field conditions better than the uniaxial test. However, the simplicity and practicability of uniaxial test have made it the most widespread test for determining the rutting response of the material (Figure 2-5).

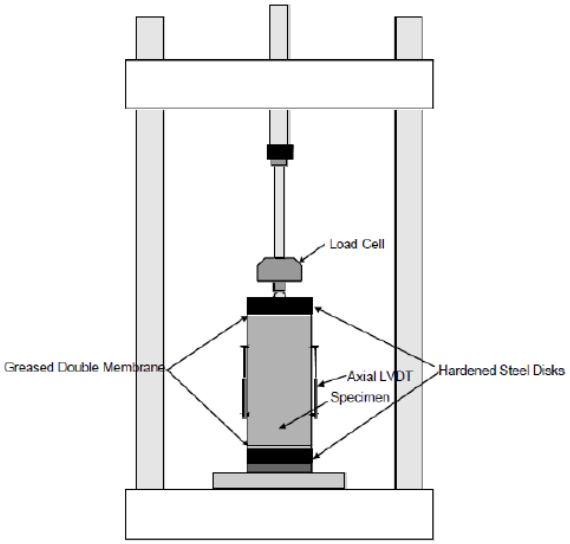

Figure 2-5: Schematic of the Permanent Deformation Test Setup [23]

Asphalt mixture rutting is believed to be a creep phenomenon. Based on laboratory testing results, an asphalt mixture subjected to a repeated load, shows three different creep response stages: primary, secondary, and tertiary (Figure 2-6). In the primary zone, the strain rate rapidly decreases to a constant rate; in the secondary zone, the strain rate is constant up to

tertiary zone; and in the tertiary zone, the strain rate increases rapidly, leading to complete failure of the asphalt mixture structure (Figure 2-7).

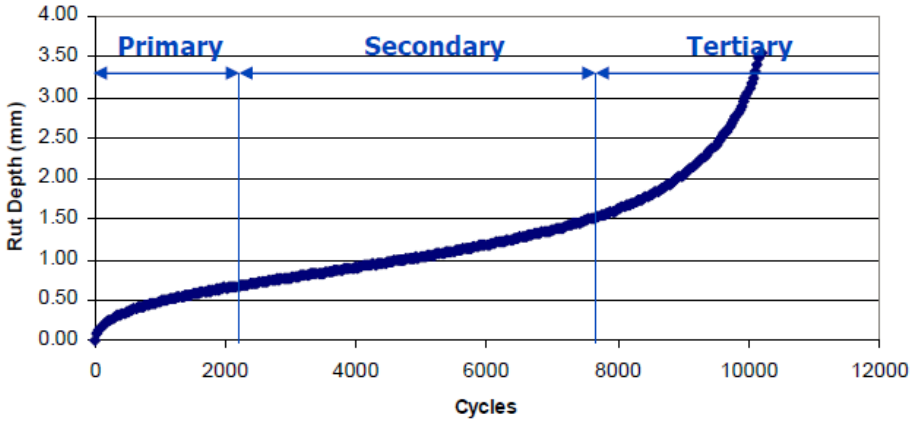

Figure 2-6: General Description of Rutting Test Result

Figure 2-7: Observed macro-cracking on an asphalt mixture sample [24]

Zhou and Scullion (2002) described the physical damage processes for asphalt mixture during the primary, secondary, and tertiary zones of rutting as strain hardening (or micro-flow), micro-cracking occurrence and propagation, and macro-cracking occurrence and propagation [25]. They concluded that from the rutting point of view it is not necessary to characterize the

tertiary zone in rutting models as it is more related to fatigue cracking properties of the asphalt mixture.

Roohi et al. (2012) studied the rutting behavior of hot mix asphalt in different zones of rutting. Internal Structure Index (ISI) is a parameter defined in that study which shows the level of connectivity of the aggregates inside of the mixture [15]. Based on their findings, the internal structure index mostly controls the asphalt mixture rutting resistance after the primary zone (Figure 2-8), while the asphalt binder's role in rutting performance of asphalt mixture is mostly in the primary zone of rutting.

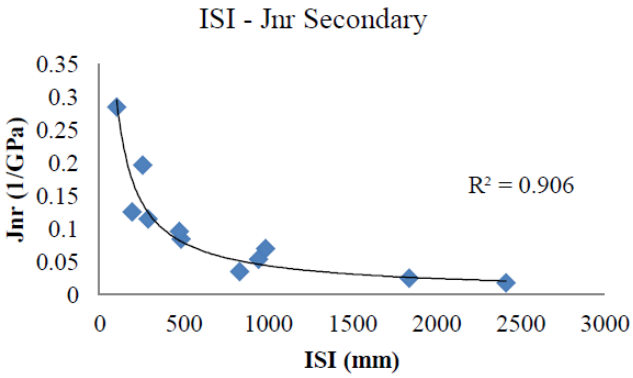

Figure 2-8: Non-recoverable creep compliance vs. ISI [15]

The reviewed studies indicate that in order to investigate the effect of binder properties on rutting, the primary and secondary zones must be studied.

2.4 Image Analysis

Visualization of components is a process that has helped many industries understand components they produce or utilize and has brought tremendous benefits to many fields, especially in the medical field. In the field of asphalt paving there has been significant attempts to utilize this

technique to better understand HMA behavior, especially for modeling the material response and behavior.

Digital images obtained from the asphalt mixtures are analyzed to quantify internal structure properties of the mixes included: contact zone properties, aggregate segregation, and aggregate orientation [15]. Those images can be captured using destructive or non-destructive methods. In the destructive method the sample should be cut in horizontal or vertical directions to provide a smooth surface for flatbed scanners (Figure 2-9). X-ray computed tomography (XRT) is a non-destructive imaging method, capable of capturing 2D or 3D image of the internal structure of an asphalt mixture sample (Figure 2-10). The planar x-rays from different directions pass through the material and are captured by a detector. Attenuations of x-rays may be recorded to identify different components of the asphalt mixture and their spatial location. After finishing the collection of x-ray attenuations for a full rotation, the sample is moved downward for scanning the next level [26].

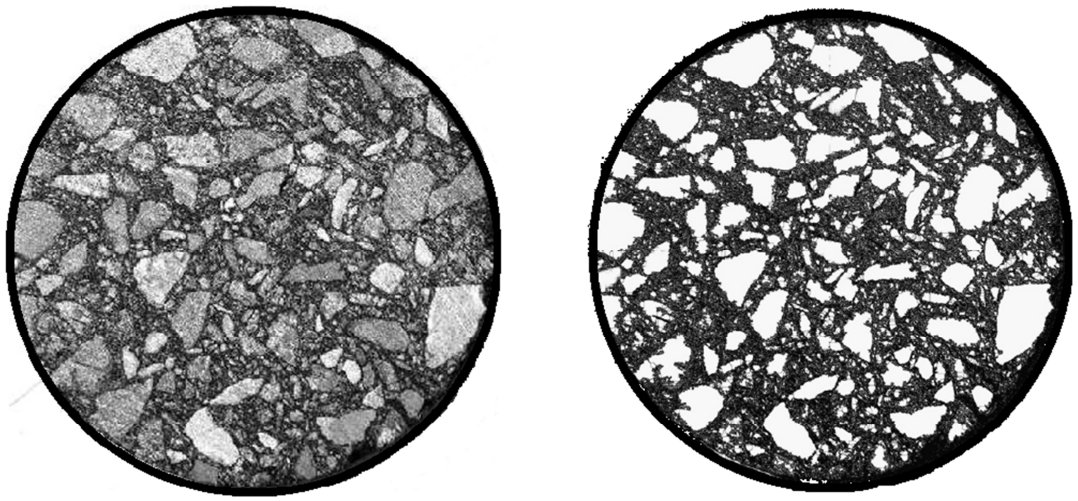

Figure 2-9: (a) A horizontal plane section taken from a pavement core (b) Resulting binary image (Bruno et al., 2011)

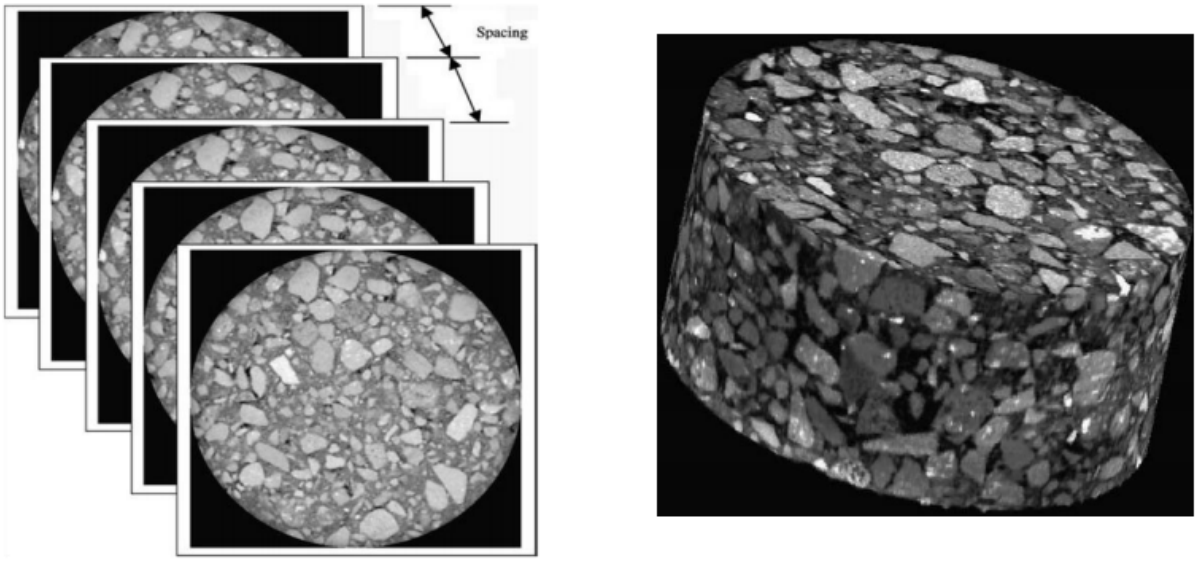

Figure 2-10: (a) Cross-sectional images produced by XRT imaging (b) Visualization in 3D of an asphalt concrete specimen [26]

X-Ray Tomography and 2D scanning has become very common in research, but challenges regarding how much one can visualize and the tremendous cost of x-ray tomography are still being phased. Thus currently researchers have been attempting to enhance accuracy of images in represent HMA components and thus make 2D visualization a more effective tool.

2.5 Finite Element Analysis

The first comprehensive presentation of Finite Element Method (FEM) is attributed to Turner et al (1956). Since its beginning many researchers used this method and the literature on this topic has increased exponentially [27, 28, 29].

Finite element analysis is based on discretizing the domain of the problem to smaller subdomains (elements). Based on the nodal displacements of an element, one can obtain the displacements, strains, and stresses over the area or volume of that element. The strain and nodal displacement relation is given in Equation 2.1:

$$\{\boldsymbol{\epsilon}\} = [\boldsymbol{B}]\{\boldsymbol{U}\} \tag{2.1}$$

where, **ε** is the strain vector; **B** is a matrix of linear operators (derivatives of shape functions) and **U** is nodal displacement vector. The element stiffness matrices are calculated using:

$$\boldsymbol{K}^e = \int \boldsymbol{B}^T \boldsymbol{D}\boldsymbol{B} dv \tag{2.2}$$

where **D** is the constitutive matrix. The element stiffness matrices should be assembled into the overall stiffness matrix. The resulting system of equations (Equation 2.3) should be solved for unknown nodal displacements.

$$\boldsymbol{K}\boldsymbol{U}^q = \boldsymbol{F} \tag{2.3}$$

where **K** is the overall stiffness matrix; $\mathbf{U}^q$ is the nodal displacement vector; and **F** is the equivalent nodal force element. One can recover the stresses and strains from the nodal displacements.

Although experimental testing can obtain the macro-mechanical behavior of asphalt concrete, it is time consuming and costly to investigate the micro-mechanical response of the asphalt mixture in a laboratory due to difficulties in controlling the microstructural features such as: aggregate shape, gradation, and volume fraction. It has been proven that finite element method (FEM) is a suitable technique for application to complex constitutive behaviors and microstructure geometries pavement problems [29, 30, 31].

Chen et al. (1990) used the FE analysis software, ABAQUS, to study the effect of heavy axil load on performance of asphalt mixtures [32, 33]. They showed that the asphalt layers show more tensile strain under the uniform pressure than the un-uniform pressure. In another study, Helwany et al. (1998) used 3D FE analysis and indicated that the tensile strains at the bottom of

Asphalt Concrete (AC) layer are very sensitive to the load speed and only longitudinal strains at top and bottom of AC layer were sensitive to tire pressure [34].

Dai et al. (2006) used a mixed FE approach to study the behavior of asphalt mixtures by using rigid elements and continuum elements for aggregates and asphalt mastics, respectively [35]. By using Schapery's nonlinear viscoelastic model, a unified approach for the rate-dependent and rate-independent damage behavior was developed. To incorporate the linear and damage-coupled viscoelastic constitutive behavior of asphalt mastic, the properties of the continuum elements were specified through a user material (UMAT) subroutine within the ABAQUS code.

Abu Al-Rub et al. (2011) indicated that the effects of aggregate shape, aggregate distribution, and aggregate volume fraction should be considered in modeling the behavior of asphalt mixtures [36]. A thermodynamic-based constitutive model which couples nonlinear thermo viscoelasticity, thermo-viscoplasticity, and thermo-viscodamage behavior of asphalt mixtures was used in the study [37]. This model has been implemented in commercial FE software via UMAT.

Three dimensional (3D) finite element can solve all of the problems solved with the two dimensional (2D) finite element. However, using 3D finite element is expensive in terms of computational time and data preparation. Asphalt pavement has a large dimension in comparison with to the other dimensions; therefore, one can use 2D plane strain condition instead of 3D modeling for this problem. Hua (2000) compared 2D and 3D finite element results of pavement rutting [38]. Figure 2-11 shows the surface profile obtained from 2D and 3D FE modeling. As it can be seen the difference between 2D and 3D results is not significant. The maximum

difference of rut depth between the two models is less than 2%. Therefore, 2D plane strain FE modeling of asphalt pavements is reasonable and has been used in this study.

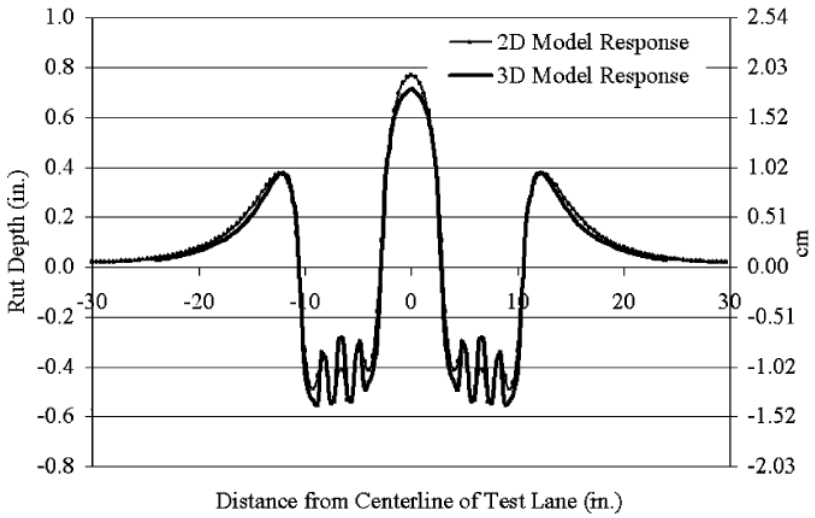

Figure 2-11: Comparison of 2D and 3D model responses [38]

2.6 Multi-scaling

Aggregate particles used in pavements typically have irregular shapes and varying sizes, ranging from less than 1μm up to 50mm. Simulation of such a material with numerical methods requires tremendous computational cost [39]. The search for an accurate analysis method which can account for the microstructure of the mixture at a reasonable computational cost has led researchers to the multi-scale modeling approach. This method has gained considerable popularity in different fields of mechanics in recent years [40, 41, 42, 36].

Yin et al. (2011) showed that multi-scale modeling can reduce the cost of the computation by reducing the amount of elements in the numerical model. They indicated that one can achieve a balance between the efficiency of the numerical solution and its accuracy by using multi-scale modeling.

The up-scaling approach is presented in this study to relate the macro-scale behavior of asphalt mixture to rheological properties of asphalt binder. In the multi-scale approach, each scale is modeled heterogeneously to determine the bulk material response properties at the analyzed scale. If statistical homogeneity at the analyzed scale has been satisfied, the properties calculated at that scale are then inputted into a homogeneous matrix at the next-higher level (Figure 2-12).

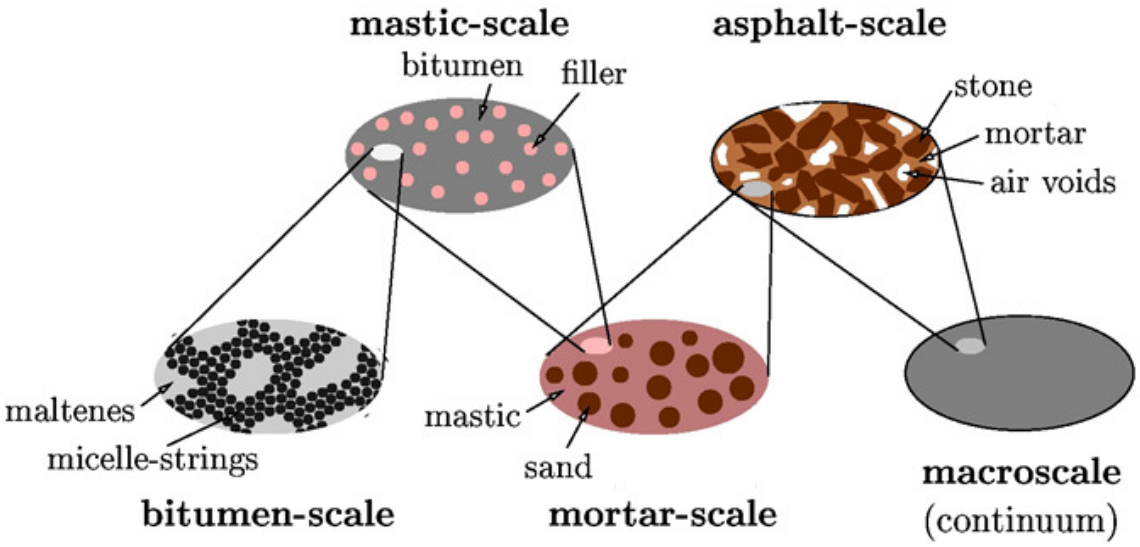

Figure 2-12: Multi-scale model with four additional observation scales below the macro-scale [40]

Lutif et al. (2009) used an efficient multi-scale computational method to simulate the mechanical response of asphalt mixtures, showing that this approach can significantly reduce the computational effort compared to single scale modeling [39]. Aigner et al. (2009) showed that good agreement can be achieved between results from multi-scale models and experimental results [40].

According to Wang (2011), multiscale modeling techniques have been improved significantly and they have reached a point where they may help researchers in selecting the materials, developing mix design, and characterizing mixture properties more accurately [43].

2.7 Main Conclusions

Based on reviewed literature in the previous sections, these main conclusions were made:

- Modifiers are used to improve one or more of binder's basic properties.
- In case of angular aggregates, the effect of binder modification is comparable with effect of gradation.
- Development of permanent deformation in asphaltic layer of hot mixt asphalt (HMA) is directly related to the stress distribution in the binder phase of the asphalt mixture.
- Shear deformation is the primary rutting mechanism in the asphalt mixtures.
- Effect of binder elasticity and stiffness on rutting performance of asphalt mixture is not understood.
- Rutting performance of asphalt mixture in the secondary zone is mostly dependent of aggregate structure inside of the mixture.

3. Methods and Material

3.1 Image Analysis Overview

A flatbed scanner was used to capture color images at a resolution of 20 μm/pixel of HMA cross sections. Two dimensional digital image processing techniques were used to convert the color images to binary images following filtering procedures described by Coenen et al (2011) using the image processing software iPas, later modified to iPas2 by Roohi et al. (2012) [15, 44]. The software uses a three step filtering procedures to generate binary images consisting of watershed filtering, thresholding and hybrid max filtering, details of which can be found elsewhere [15, 44]. This software can be used to perform a micro-structural analysis on 2D images and quantify the internal structure of the mixtures by some parameters such as number of contact points and total contact length. The imaging techniques used in this software cannot accurately capture aggregates smaller than 1.18 mm, mostly due to a portion of imaged particles smaller than 1.18 mm being lost during the application of filters when converting to binary. Therefore, a MATLAB code [45] was used to eliminate the aggregates smaller than 1.18 mm from the images (Figure 3-1), and instead including this size range in the mortar scale.

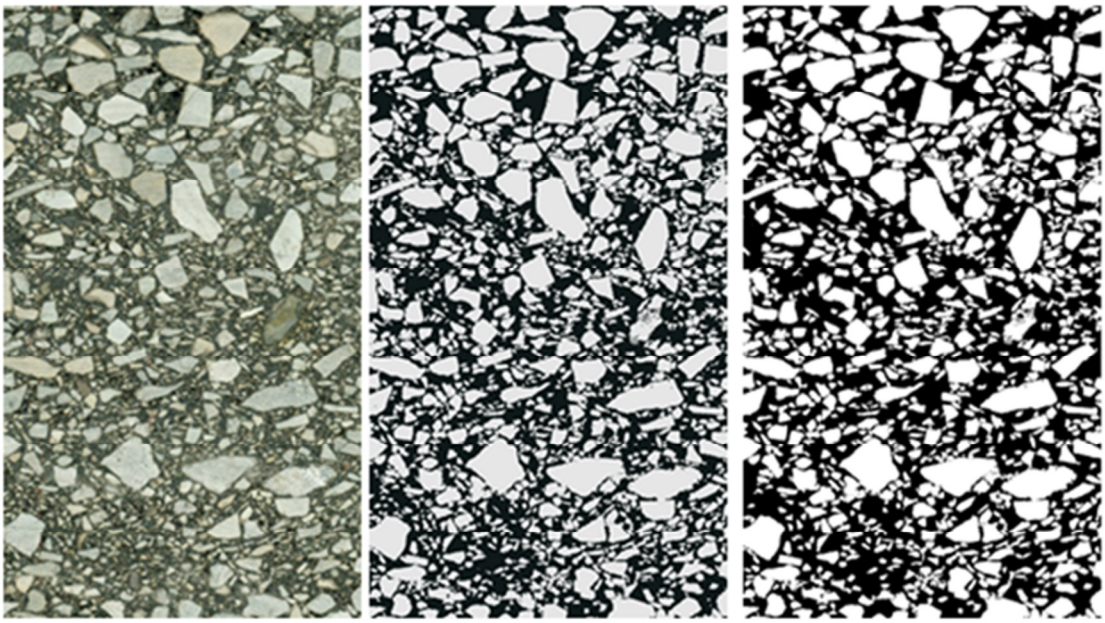

Figure 3-1: Images of the mixture. (a) Scanned image of HMA section (b) Scanned image after image filtering processes (c) Scanned image after elimination of aggregates smaller than 1.18 mm

Common imaging techniques are not capable of accurately capturing aggregate particles smaller than 1.18 mm due to a combination of factors including insufficient resolution, obscuring of fine particles during the cutting process, and imaged particle loss during application of filters when converting to binary. To address these issues the "mortar-scale" was defined to incorporate the fine aggregates under 1.18 mm and above 0.075 mm. A code was written in the MATLAB v7.12 platform to generate mortar aggregates according to the inputted gradation and their shape by a random selection of particles from a database of fine aggregates, as will be discussed [45].

3.2 Finite Element Analysis Overview

In this study asphalt mixture was considered at four interconnected scales: the binder scale, the "mastic-scale" which contains fillers ranging from 1µm up to 75µm in a binder matrix; the "mortar-scale" containing fine aggregates ranging from 75µm to 1.18mm in a mastic matrix, and

the “asphalt mixture-scale” which contains all larger aggregates in a continuous mortar matrix that can be detected using simple 2D scanners and binary imaging filters of the asphalt mixtures. For the mortar and mastic scales a MATLAB based program was written to randomly generate the mortar and mastic binary images based on their measured respective gradations and shapes.

The Finite Element (FE) analysis software ABAQUS v6.9.1 was used to model the studied asphalt mixtures [33]. Every pixel in the binary images was mapped into a finite element mesh and the model was implemented in the software to provide numerical solutions of the stress and strain field at different scales, assuming plane strain conditions. The assumption of plane strain conditions is most reasonable when one dimension in the modeled structure is very large in comparison to the other dimensions, as in the case of pavements. A 4-node bi-linear plane strain quadrilateral and full integration element (i.e., CPE4) was used in the simulations. Similar boundary and loading conditions were used to simulate the behavior of asphalt mixtures at the macro- and micro scale, as shown in Figure 3-2. Linear elastic properties were used to model the aggregate phase, setting the Young’s modulus and Poisson’s ratio to 25000 MPa and 0.25 respectively. Linear viscoelastic behavior was used for the binder phase, assuming a constant Poisson’s ratio of 0.49. Similar values have been used for modeled pavement material properties in the literature [29, 36].

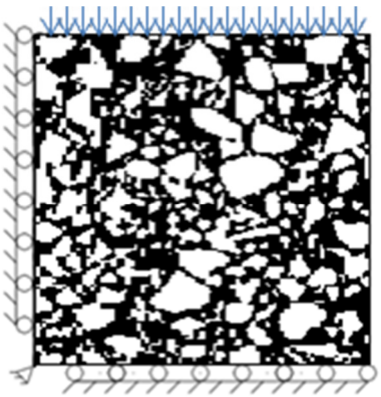

Figure 3-2: 2D asphalt mixture model showing loading and boundary condition

3.3 Multi-scaling Approach

Multi-scale modeling relates the behavior of the modeled material at the macro-scale to the micro-scale properties and behavior (Figure 3-3). Throughout the analysis, material properties are calculated at the finest scale and progressively shifted to the next-higher level [40]. The Representative Area Element (RAE) is defined at every scale to determine the appropriate model geometry. In the multi-scale approach, each scale is modeled heterogeneously to determine the bulk material response properties at the analyzed scale. The properties calculated at each scale are then inputted into a homogeneous matrix at the next-higher level.

The continuous matrix in the mortar phase consists of homogenized "mastic-scale" elements. The mastic-scale, consisting of mineral filler and binder, was modeled similar to the mortar-scale, using the aforementioned MATLAB code to generate the filler distribution using filler gradation curves measured by Laser Diffraction methodology and by selecting the particles from a database of filler shapes obtained by an electron microscope (Figure 3-4).

The optimum RAE size was determined for each scale based on the convergence of their viscoelastic properties, as will be explained in greater detail in later sections. Experimentally derived binder material properties were inputted into the mastic scale model, completing the multi-scale model representation of the asphalt mixture, as shown in Figure 3-3.

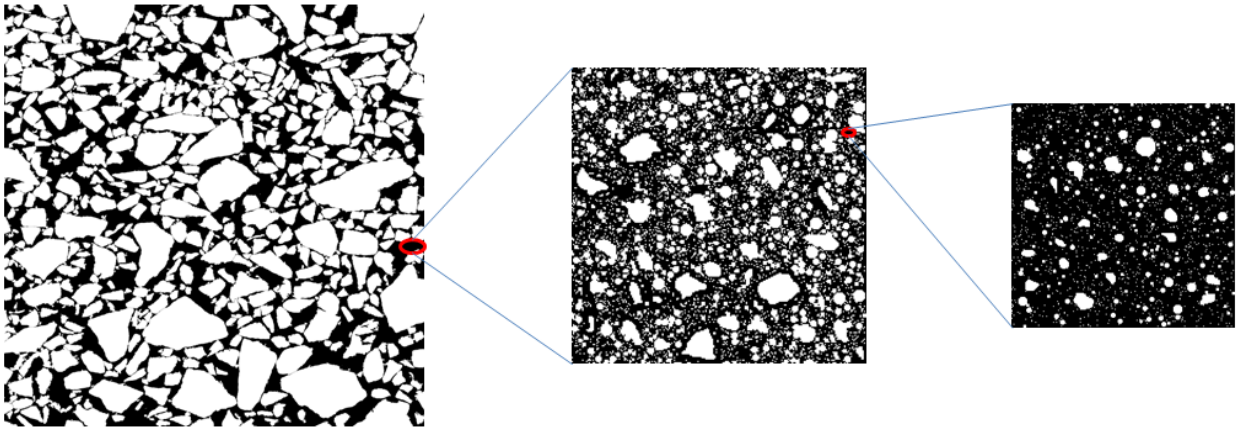

(a) (b) (c)

Figure 3-3: Multi-scale analysis scheme: (a) Asphalt-scale (large aggregates in mortar matrix) (b) Mortar-scale (fine aggregates in mastic matrix) (c) Mastic-scale (fillers in binder matrix)

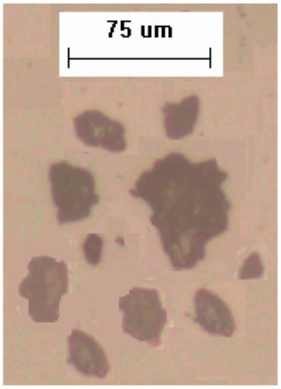

(a)

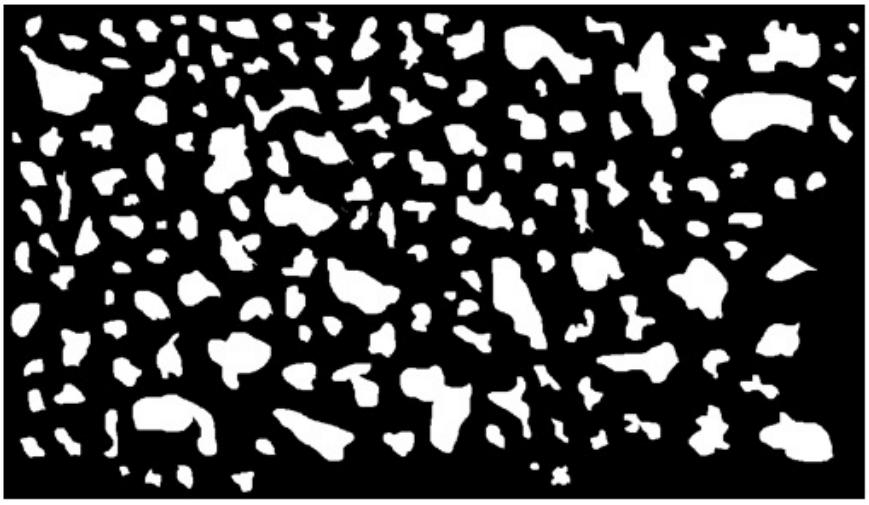

(b)

Figure 3-4: (a) Scanned microscopic image of granite stone fillers (b) Database of filler shapes

Three asphalt mixtures with widely different gradations, categorized as fine, intermediate and coarse, were used in this study, as shown in Figure 3-5. Mixture volumetric properties were kept constant for all three gradations. Asphalt content was 5.1% by weight (13.0% by volume), and air void content was 7% by volume. Consequently approximately 80% of the asphalt mixtures by volume would be constituted of aggregate. Figure 3-6 shows the scanned images of the three mixtures used in this study, while Table 3-1 shows the volume fraction of the components at each scale. In the following sections the development of each scale and input value derivation methodology is described in greater detail and analysis results are discussed.

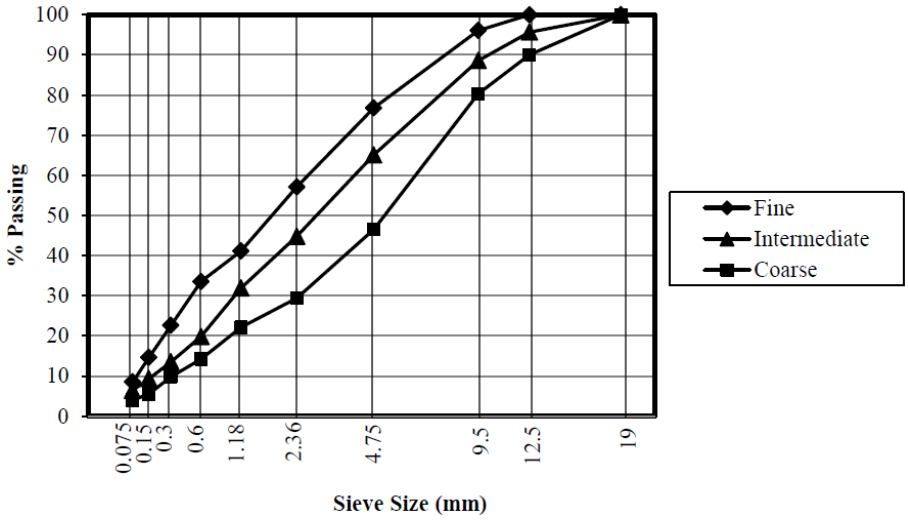

Figure 3-5: Gradation of mixtures

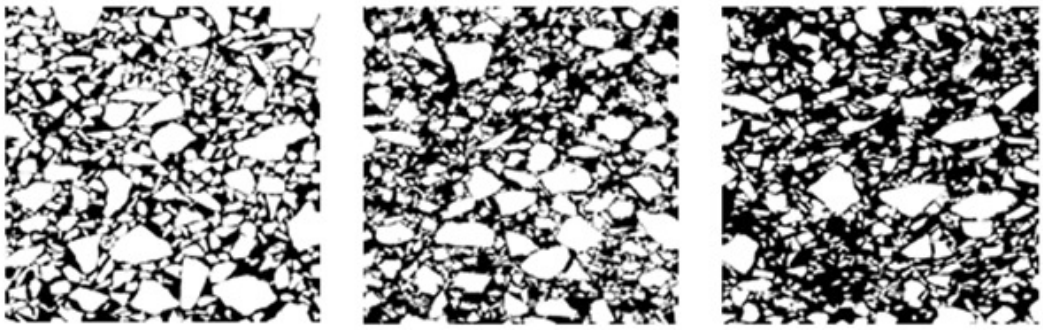

Figure 3-6: Scanned images of the mixtures (a) Coarse (b) Intermediate (c) Fine

Table 3-1: Volume fraction of components at each scale

Scale / Mixture	Asphalt Scale			Mortar Scale		Mastic Scale	
	Aggregates	Mortar	Air Void	Fine Aggregates	Mastic	Fillers	Binder
Coarse	0.66	0.30	0.04	0.45	0.55	0.20	0.80
Intermediate	0.58	0.38	0.04	0.50	0.50	0.30	0.70
Fine	0.49	0.47	0.04	0.55	0.45	0.40	0.60

Two groups of artificial binders were used to study the binder elasticity and binder viscosity effect on rut resistance of asphalt pavement. In the first group four artificial binders with the same viscosity (permanent deformation) but different levels of instantaneous elasticity and delayed elasticity were used to study the binder elasticity effect on rutting behavior of asphalt mixtures: (1) High Instantaneous elastic response and High Delayed elastic response (HIHD), (2) High Instantaneous elastic response and Low Delayed elastic response (HILD), (3) Low Instantaneous elastic response and High Delayed elastic response (LIHD), and (4) Low Instantaneous elastic response and Low Delayed elastic response (LILD) (Figure 3-7). As shown, all binders resulted in the same permanent deformation.

In the second group, four artificial binders with two levels of viscous component (permanent deformation) and two levels of elastic component were used to compare the binder viscous and elastic properties effect on asphalt mixture rutting: (1) High Viscous component binder with Low Recovery (HVLR), (2) Low Viscous component binder with Low Recovery (LVLR), (3) High Viscous component binder with High Recovery (HVHR), and (4) Low Viscous component binder with Low Recovery (LVLR) (Figure 3-8).

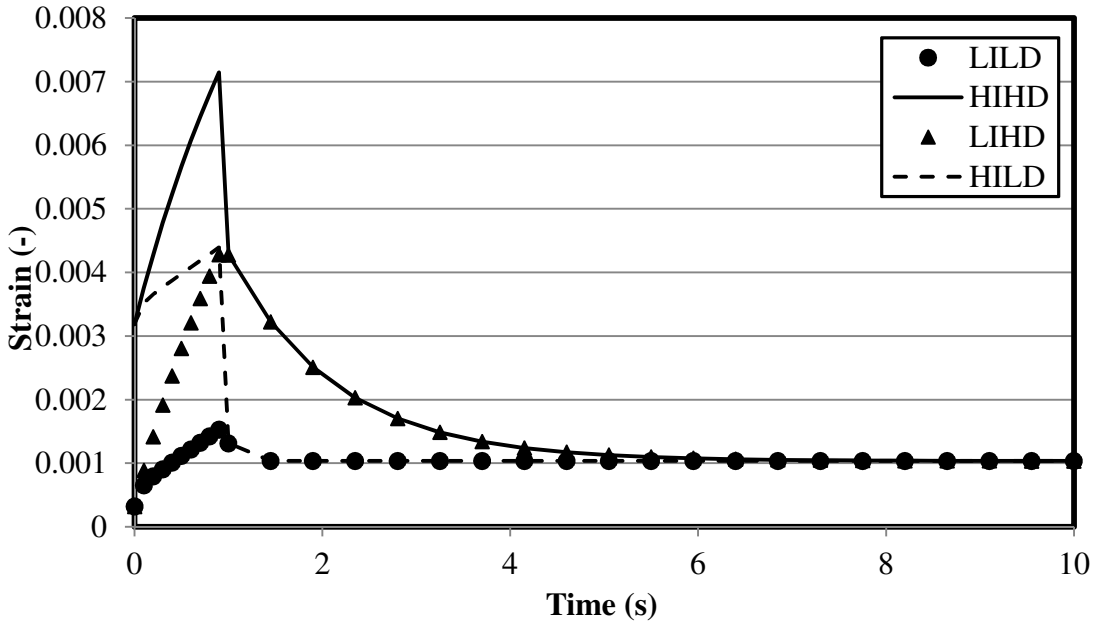

Figure 3-7: Creep and recovery diagrams of first group of binders

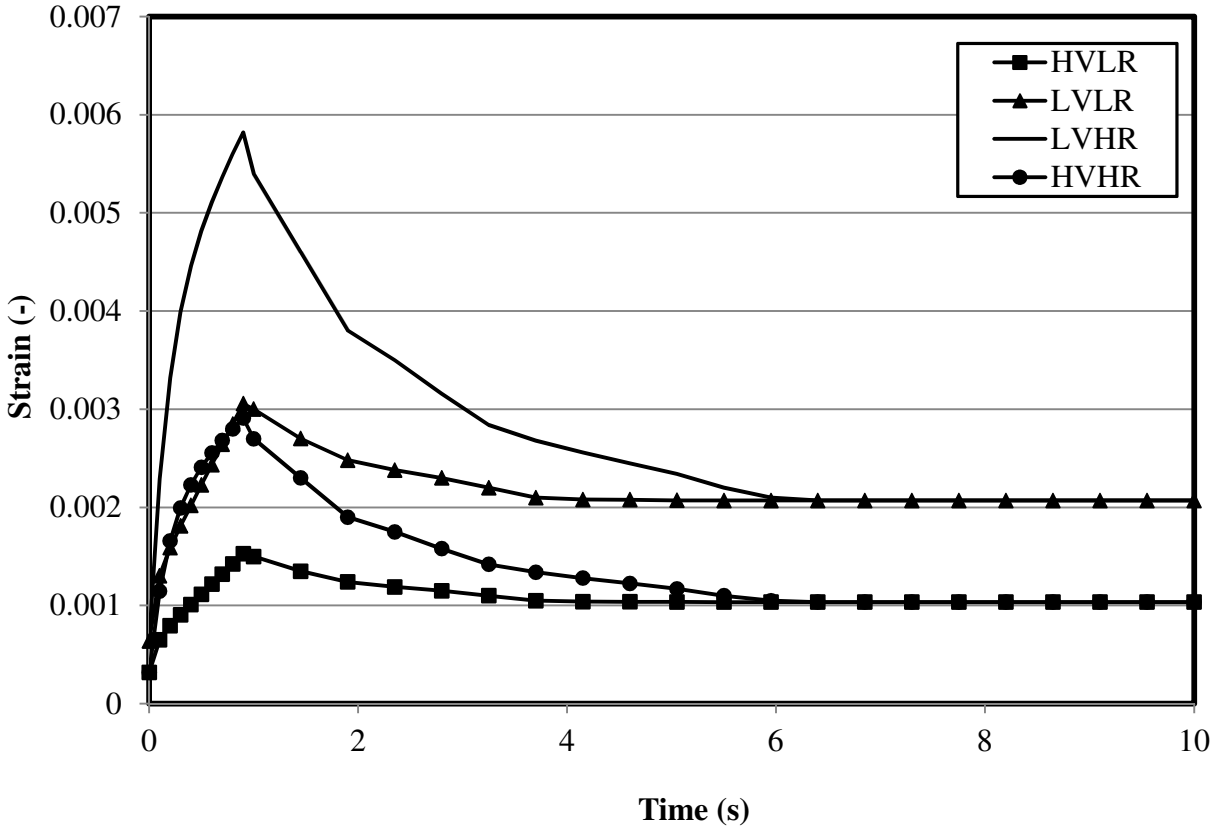

Figure 3-8: Creep and recovery diagrams of second group of binders

3.3.1 Binder Scale

As mentioned previously, the binder phase in multi-scale model was assumed to be describable by the principals of linear viscoelasticity for the purpose of the analysis in this study. Linear viscoelastic behavior is defined in ABAQUS using a relaxation modulus Prony series form as shown in (3.1).

$$E(t) = E_\infty + \sum_{i=1}^{n} E_i e^{\frac{-t}{\tau_i}} . \quad (3.1)$$

In which:

- $\boldsymbol{E_\infty}$ is the long term modulus
- $\boldsymbol{E_i}$ is the Prony series normalized relaxation modulus
- t is loading time, and
- $\boldsymbol{\tau_i}$ is relaxation time

The parameters of the Prony series were determined by converting experimentally derived binder creep compliance values to relaxation modulus. The experimental values were measured through creep and recovery testing using a Dynamic Shear Rheometer (DSR) following the multiple stress creep and recovery procedure (MSCR) (AASHTO TP 70). The creep compliance was determined by fitting a Burger's model (Figure 3-9) to the experimental data.

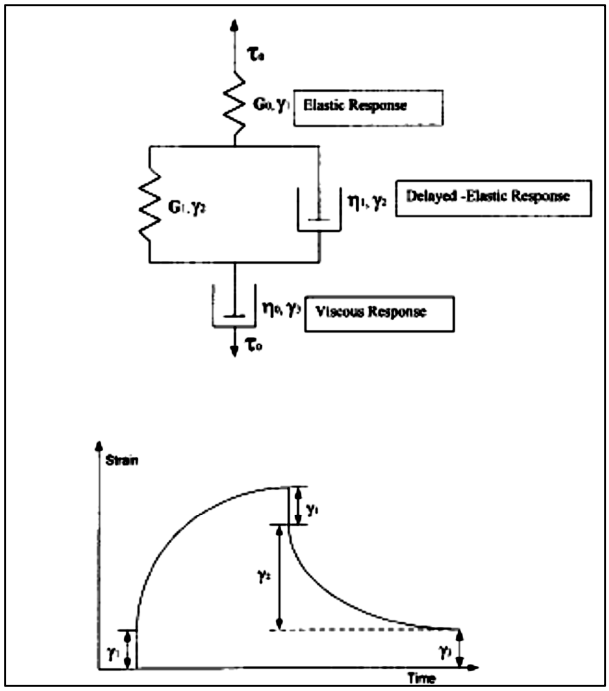

Figure 3-9: Burger's Model and its response [6]

Burger's model is a combination of a Kelvin model and a Maxwell model as shown in Figure 3-10. The Kelvin part and the spring of the Maxwell part are representatives of the elastic behavior of asphalt binder. The representative of viscous properties of the asphalt binder is the dash-pod (viscous damper) in the Maxwell part as well. In the first group of binders where the effect of binder elasticity is studied on rut resistance of asphalt mixtures, the viscous properties of the asphalt binders are the same by keeping the dash-pod component the same in all binders. In these binders initial elastic response and delayed elastic response of the binders were changed by using two different levels for the springs constants. As it was mentioned earlier in the second group of binders two levels of elasticity and two levels of viscosity are considered. Binder elasticity levels have been changed by assuming two levels for the spring constants of the Kelvin part and keeping the dash-pod of the Kelvin part and the spring of the Maxwell part unchanged.

Binder viscosity levels are considered by assuming two levels for the dash-pod of the Maxwell part (Table 3-2 and Table 3-3).

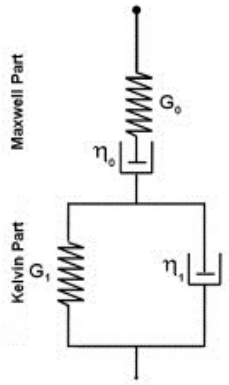

Figure 3-10: Burger's model: A Kelvin element in series with a Maxwell element

Table 3-2: Burger's Model Parameters of the first binder group

Parameter / Binder	Em	η m	Ek	η k
LILD	3.14E+05	9.66E+04	3.60E+05	2.05E+04
LIHD	3.14E+05	9.66E+04	1.80E+04	2.05E+04
HILD	3.14E+04	9.66E+04	3.60E+05	2.05E+04
HIHD	3.14E+04	9.66E+04	1.80E+04	2.05E+04

Table 3-3: Burger's Model Parameters of the second binder group

Parameter / Binder	Em	η m	Ek	η k
HVLR	3.14E+05	9.66E+04	3.60E+05	2.05E+04
HVHR	3.14E+05	9.66E+04	3.60E+04	2.05E+04
LVLR	3.14E+05	4.80E+04	3.60E+05	2.05E+04
LVHR	3.14E+05	4.80E+04	3.60E+04	2.05E+04

Creep compliance in expressed by (3.2) for material following Burger's model behavior.

$$J(t) = \frac{1}{E_m} + \frac{t}{\eta_m} + \frac{1}{E_k}\left(1 - e^{-\frac{E_k}{\eta_k}t}\right) \tag{3.2}$$

In which:

- E_m is the instantaneous modulus (spring element in series)
- E_k is the delayed elastic modulus (spring element in parallel)
- *t* is loading time, and
- η_m and η_k are dashpot viscosities in series and in parallel, respectively.

The constitutive equations relating viscoelastic stress to strain and modulus are referred to as the "Boltzmann superposition" integrals, as expressed in (3.3a) and (3.3b), where ε, σ and t are strain, stress and loading time, respectively; J(t) is the creep compliance, and E(t) is the relaxation modulus. By applying a Laplace transformation to (3.3a) and (3.3b), manipulation of terms, and a subsequent inverse Laplace transformation, one may convert and rewrite the Burger's model creep compliance in terms of the relaxation modulus Prony series to be inputted into ABAQUS. The procedure is shown below, in equations (4.3) to (7.3c).

$$\epsilon(t) = \int_0^t J(t-\tau)\frac{d\sigma(\tau)}{d\tau}d\tau, \tag{3.3a}$$

$$\sigma(t) = \int_0^t E(t-\tau)\frac{d\varepsilon(\tau)}{d\tau}d\tau, \tag{3.3b}$$

$$E(s) = \frac{1}{s^2 J(s)} = \frac{P_1 s + P_2}{Q_1 s^2 + Q_2 s + Q_3}, \tag{3.4}$$

Where:

$$P_1 = E_M \eta_M E_K, \tag{3.5a}$$

$$P_2 = \frac{E_M \eta_M {E_K}^2}{\eta_K}, \tag{3.5b}$$

$$Q_1 = \eta_M E_K, \tag{3.5c}$$

$$Q_2 = \frac{\eta_M {E_K}^2}{\eta_K} + E_M E_K + \frac{E_M \eta_M E_K}{\eta_K}, \tag{3.5d}$$

$$Q_3 = \frac{E_M {E_K}^2}{\eta_K}. \tag{3.5e}$$

The Laplace inverse transform is applied to the above equation, so:

$$E(t) = E_1 e^{s_1 t} + E_1 e^{s_1 t}, \tag{3.6}$$

With:

$$s_1, s_2 = \frac{-Q_2 \mp \sqrt{{Q_2}^2 - 4Q_1 Q_3}}{2Q_1}, \tag{3.7a}$$

$$E_1 = \frac{E_M}{s_1 - s_2}\left(\frac{E_K}{\eta_K} + s_1\right), \tag{3.7b}$$

$$\boldsymbol{E_2 = E_M\left(1 - \frac{\frac{E_K}{\eta_K} + s_1}{s_1 - s_2}\right)}. \tag{3.7c}$$

Equation (3.6) shows the relaxation modulus of the Burger's model in the form of a Prony series, formatted according to ABAQUS input requirements. Figure 3-11 shows that the Burger's model can predict the behavior of the asphalt binder under creep loading accurately. This model was implemented in Finite Element (FE) model at the "mastic scale" to identify the properties at the next higher level, as will be discussed in the following sections.

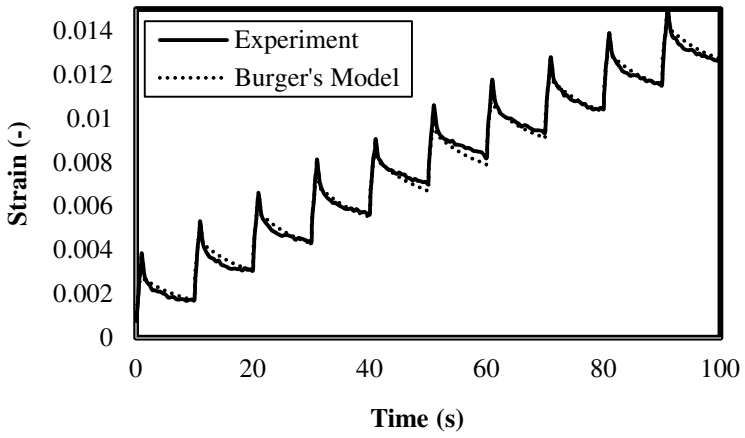

Figure 3-11: Creep and recovery diagram of a binder sample under 10 cycles of loading and unloading (Experimental results and Burger's model results)

3.3.2 Mastic Scale

To study the effect of filler gradation on the stress and strain distribution at the mastic scale, three different gradations of mineral fillers were selected: limestone gradation (LS), dolomite stone gradation (DS), and granite stone gradation (GS). The gradations for each of these mineral fillers, measured using Laser Diffraction, are shown in Figure 3-12. It can be seen that granite and limestone have rather similar gradations, while dolomite has a relatively coarse gradation. In terms of specific area this would indicate a much larger specific area for granite and limestone compared to the courser dolomite filler.

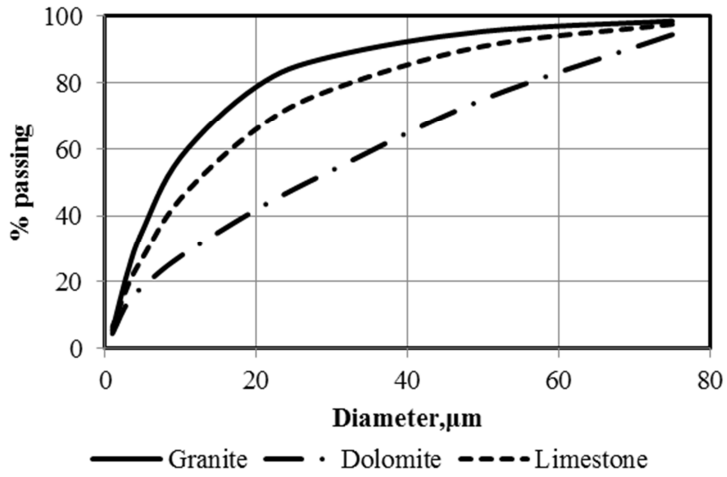

Figure 3-12: Gradation of the fillers used in present study

For generating the mastic images, the microscopic images of the fillers were made and 230 different shapes of fillers were saved in a database. The mastic generation code based on the gradation and filler volume fraction of the mastic scale which are imported by the user, choose randomly some of the filler shapes in the database and make the mastic binary image. Typical mastic images generated by the code are shown in Figure 3-13. Four different volume fractions (φ), 0.1, 0.2, 0.3 and 0.4, were used to study the effects of volume fraction on the stress distribution in the mastic scale binder phase. In terms of percentage of total aggregate in mixtures, based on gradation these volume fractions cover a range of approximately 2.5 to 10% passing the #200 sieve.

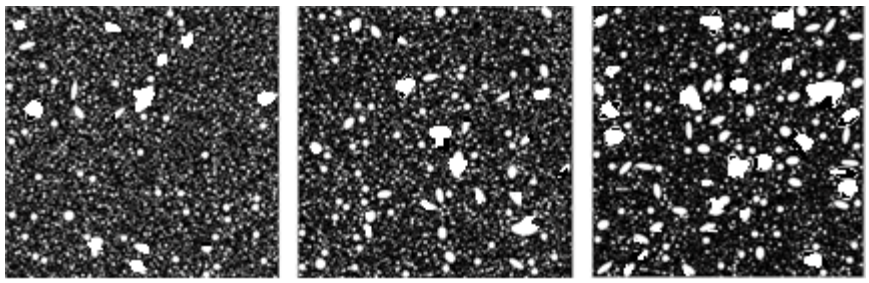

Figure 3-13: Examples of generated mastics with ϕ=0.2: (a) GS Mastic (b) LS Mastic (c) DS Mastic

3.3.3 Mortar Scale

The next higher level after the mastic scale can be called the "mortar scale", as previously discussed. This scale consists of fine aggregates, larger than 0.075 mm (#200 sieve opening) and smaller than 1.18 mm. The gradation of fine aggregates in the mortar scale is determined from the total aggregate gradation used for the mixture. The same MATLAB code as used for the mastic image generation was used at the mortar scale to generate the mortar images based on their gradation. The mortar generation code uses the shape of 100 different fine aggregates to generate the mortar scale images.

3.3.4 Asphalt Mixture Scale

The "asphalt mixture scale" is the highest level scale in the multi-scale analysis scheme used in the present study. The continuous phase of the asphalt images in this scale is formed by the mortar scale. Mortar material properties are inputted as material properties in the continuous matrix at the asphalt mixture scale, assuming an isotropic and homogeneous mortar matrix at this scale. Mortar scale properties were determined through input of mastic viscoelastic properties from the mastic scale analysis, which in turn was determined through inputting experimentally derived and analytically converted binder viscoelastic properties at the mastic scale analysis. This step by step analysis and inputting procedure completes the multi-scale simulation of the asphalt mixture, as used in the present study.

Due to the lack of color contrast between air voids and the background asphalt, coupled with the unavoidable filling of most air voids on the cut HMA surface during cutting, air voids cannot be reliably captured using the current 2D imaging techniques. In the present study it was decided to overcome this deficiency by introducing artificially generated circular air voids in the

asphalt scale image. Masad et al. (2002), studied the air void distribution in the asphalt mixtures, concluding that the air void distribution of gyratory compacted samples followed a bathtub shape distribution, such that larger air voids were located near the top and bottom of the specimens, with the air voids in central portion having a relatively consistent smaller size [46]. The same distribution was used in this study to distribute the air voids in the asphalt scale, as shown in Figure 3-14.

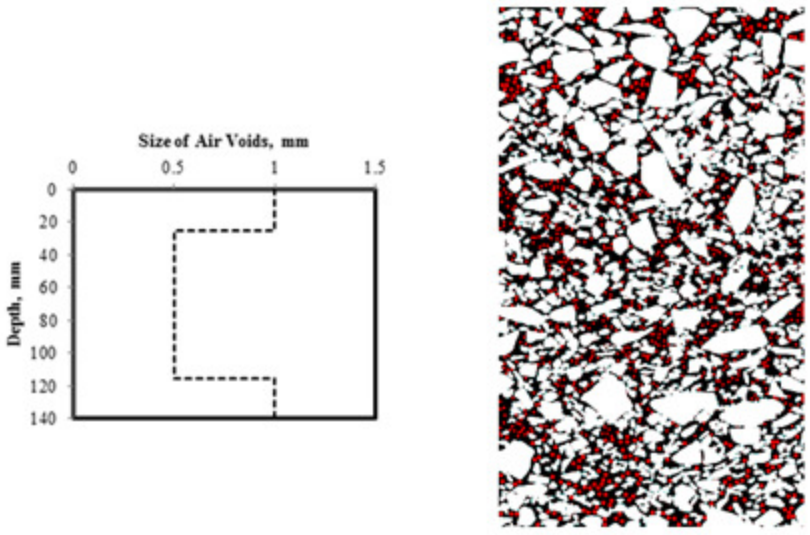

Figure 3-14: Distribution of air void sizes with depth

3.4 Simulation of Particle Contacts

As a composite material, asphalt concrete has a very complicated behavior. This complexity is dependent on aggregate gradation, orientation and number of contacts of aggregate particles, aggregate- binder interface properties, and air void distribution.

In a granular material, particles are in contact with other particles in their vicinity. In contact simulation the general goal is to calculate the contact pressure and the contacted areas on the surfaces. In such cases particle surfaces touch each other and a force normal to the contact

surface acts on each particles. Two particles can have contact in more than one portion (Figure 3-15).

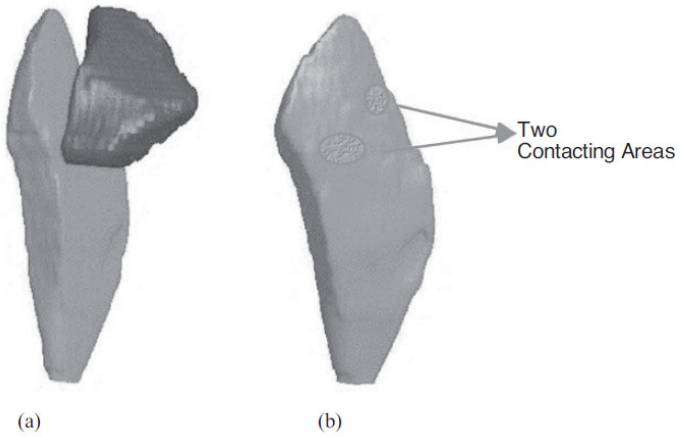

Figure 3-15: Illustration of the complexity of the contacts. (a) two contacting particles (b) particles are contacting at many points in two places [47]

Particle contacts are defined in ABAQUS by introduction of surface to surface contacts between each pair of particles. In this simulation there is no slippage for aggregates on top of each other which is thought to be the mechanism of rutting in tertiary zone (Figure 3-16).

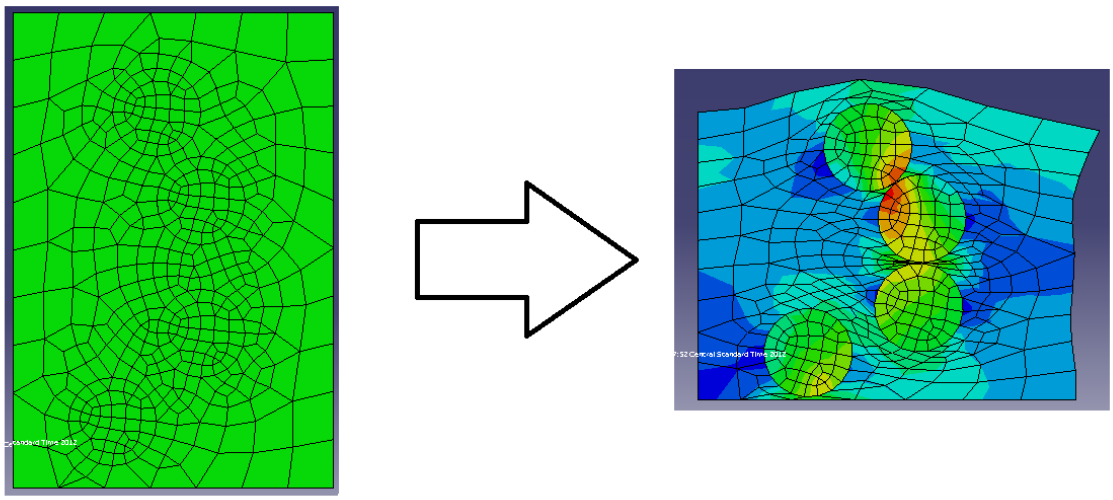

Figure 3-16: Surface to surface contact of circular particles

As it can be seen the aggregate particles are the most important load transferring component in the mixture. Also it is shown that stress concentrations happen at the contact points of the particles.

3.5 Validating Multi-scale Model

In order to confirm the validity of the multi-scale model used in this study, a coarse graded asphalt mixture with SBS modified binder and its corresponding mastic were tested in the lab and results were compared to the results obtained from the multi-scale simulation. As it is shown in Figure 3-17 there is a good agreement between the creep and recovery diagrams of the MSCR test and FEM simulation of mastic.

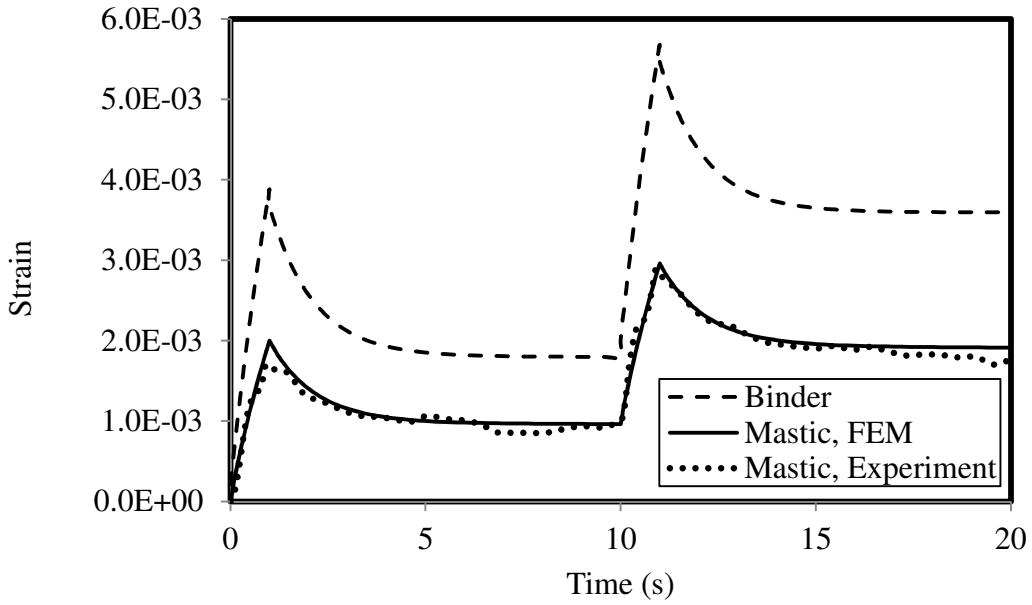

Figure 3-17: Creep and recovery diagrams of SBS modified binder and its corresponding mastic under 100 Pa compressive step stress

Material properties are calculated at the mastic scale and progressively shifted to the mortar scale. The properties of mortar scale are calculated and used as the matrix properties of

the asphalt mixture scale to obtain the overall properties of the whole asphalt mixture. As it is shown in Figure 3-18, the multi-scale model used in this study is a powerful tool capable of predicting the behavior of asphalt mixtures at small strains with acceptable accuracy. Thus the model developed in this study was used to achieve the previously defined objectives, as will be discussed in the following chapters.

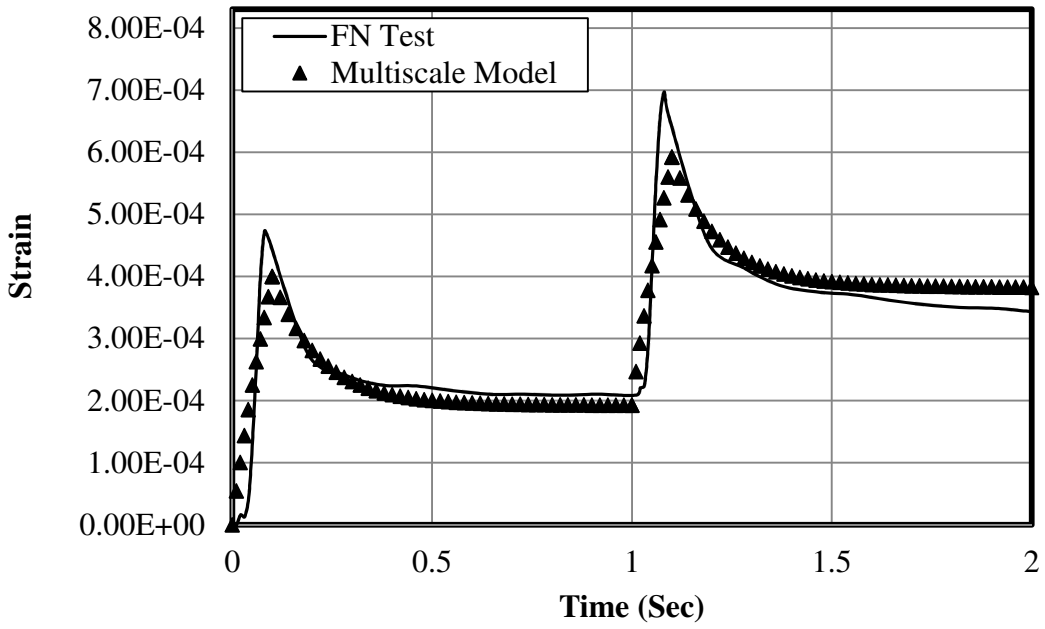

Figure 3-18: Creep and recovery diagrams of a coarse graded asphalt mixture with SBS modified binder

4. Tracking Micro-structure Changes of HMA during Rutting

Microstructural characteristics of hot mix asphalt pavements significantly changes during loading time [48]. Number of contact points of aggregates, contact length, segregation, aggregate orientation, and air void content are some these characteristics. Many researchers showed the effect of internal structure on overall performance of asphalt pavements [44, 46, 15, 48]. The focus of this chapter is on the microstructural evolution of aggregates in an asphalt mixture sample during rutting.

4.1 Methodology

In order to understand the evolution of aggregate structure in asphalt mixtures, five samples with the same volumetric properties as shown in Table 4-1 were made. The flow number test performed on two of these samples in order to distinguish the zones of rutting (Figure 4-1).

Table 4-1: Volumetric properties of the samples

NMAS	19 mm
Binder Content	5.1%
Air Void Content	7.0%

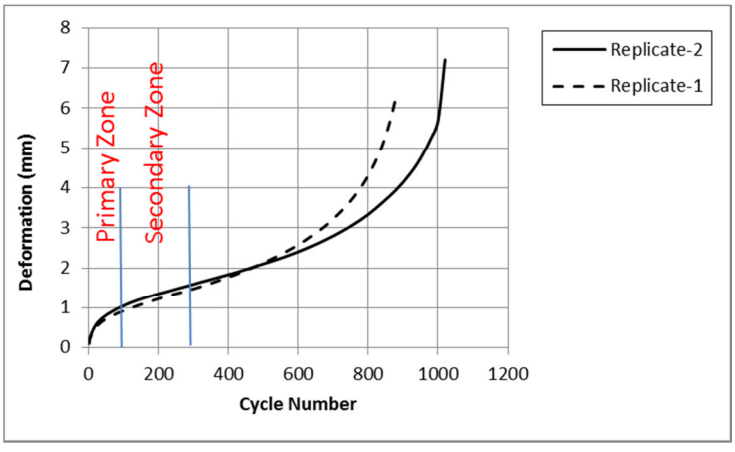

Figure 4-1: Rutting zones of the samples

As shown, the two tested sample results are in good agreement with together. Based on the results it was determined that the number of cycles to complete the primary zone and secondary zone of rutting are 100 and 260, respectively. The flow number test was performed on one of the samples and stopped after 100 cycles of loading to make sure that the sample is rutted till the end of primary zone (Figure 4-2). The test was performed on another sample and stopped after 260 cycles which is the end of the secondary zone of rutting. These samples were cut in vertical direction to provide a smooth surface for flatbed scanners. The flatbed scanner was used to capture color images at a resolution of 20 µm/pixel of HMA cross sections (Figure 4-3). The images analyzed with IPAS2 in order to determine the internal structure of the original and rutted samples.

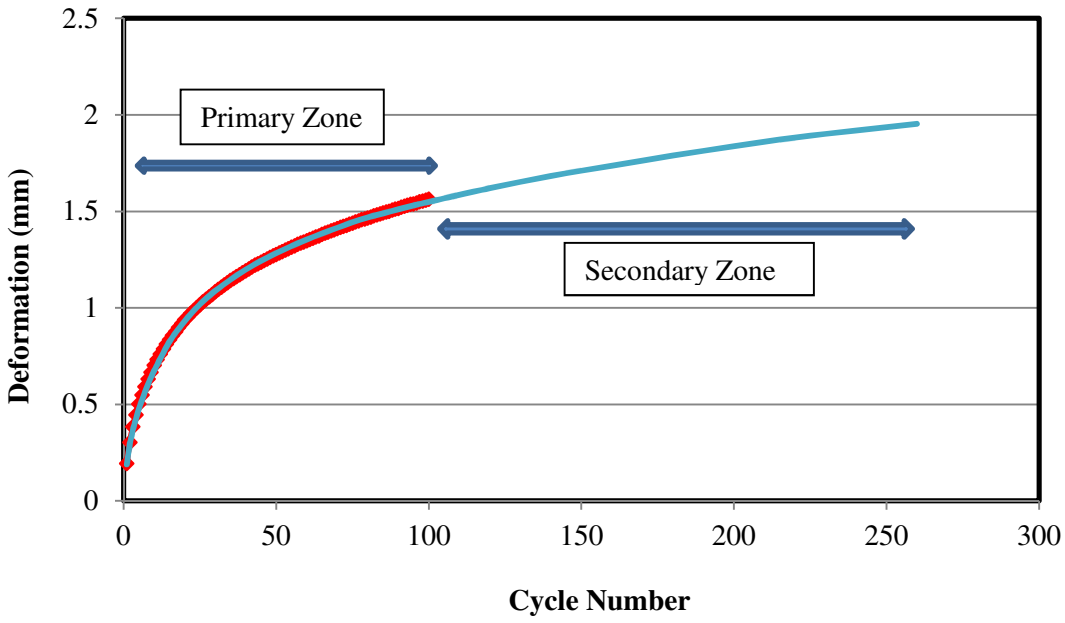

Figure 4-2: Deformation of the rutted samples

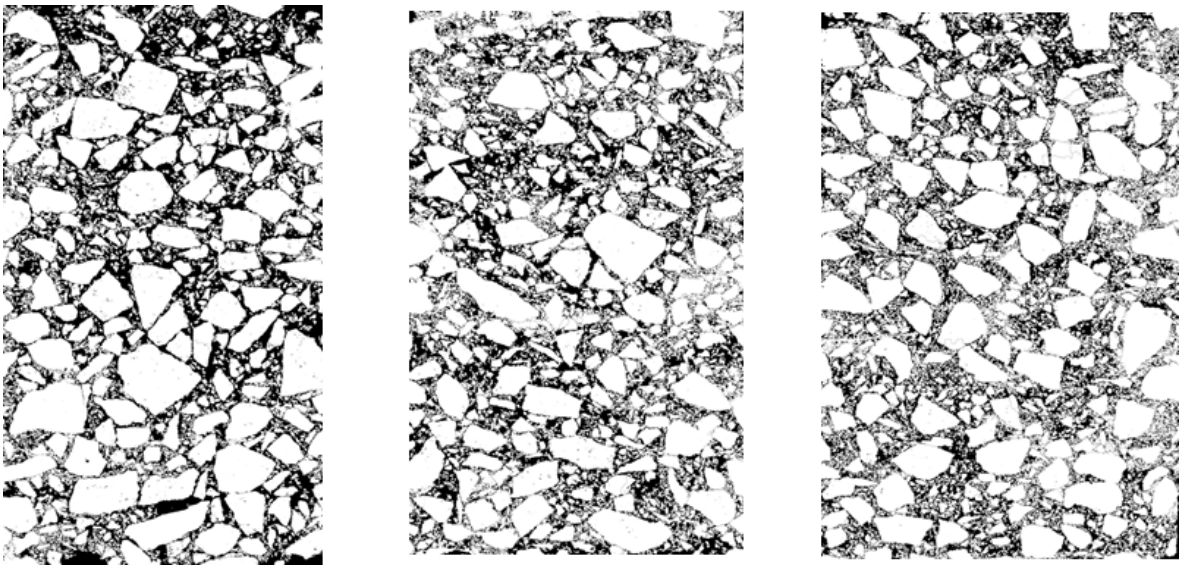

Original Sample | Rutted sample (Primary Zone) | Rutted Sample (Secondary Zone)

Figure 4-3: Scanned images of the original and rutted samples: (a) original sample (b) rutted sample till the end of primary zone (c) rutted sample till the end of secondary zone

4.2 Image Analysis Results

The scanned images of the samples were analyzed in IPAS2 and their microstructural parameters such as number of contact points and total contact length were calculated. These parameters were normalized to the area of the imaged in order to compare the results. Figure 4-4 shows that the internal structure of the asphalt mixture changes tremendously during the primary zone of rutting. It was also observed that the changing of the aggregate structure during the secondary zone is not significant.

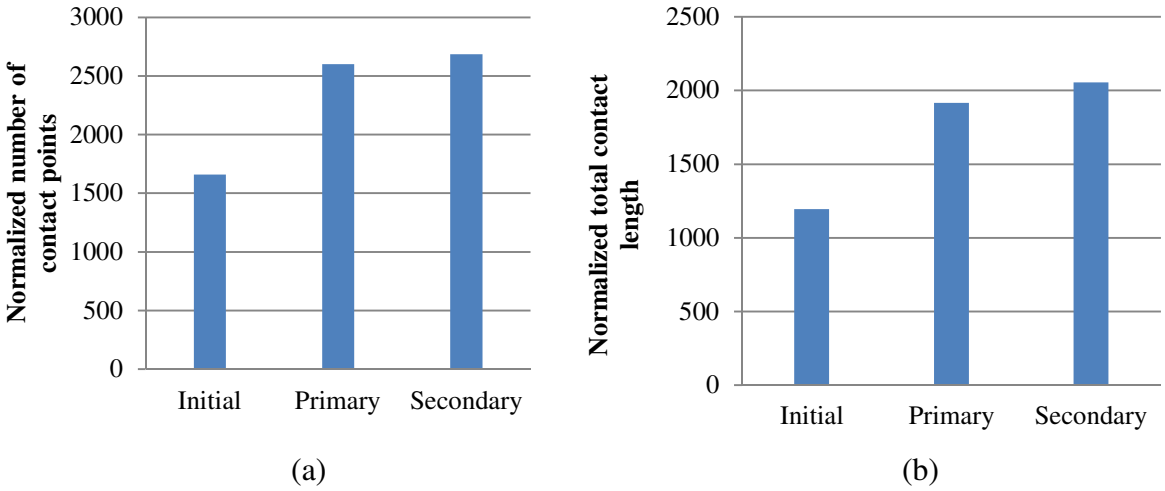

Figure 4-4: Microstructural parameters of the samples. (a) normalized number of contact points (b) normalized total contact length

These results show that in order to have an accurate simulation, the evolution of microstructure should be considered in the model. In other words changing of the contact geometry and distribution during the rutting must be taken into account.

5. Effect of Binder Properties on Rut Resistance of Asphalt Mixtures

The effect of binder properties on permanent deformation of asphalt mixtures is studied in this chapter. Using conclusions from the second chapter it was also found that the stress and strain distribution in the binder phase have a controlling role in performance of asphalt mixtures. Thus the present chapter investigates the effect of aggregate gradation and binder properties on stress and strain distribution in each scale in addition to the permanent deformation of the macro-scale.

The information available on the distribution of stress and strain in the binder phase of HMA is limited. Kose et al. (2000) analyzed digitized images using finite-element methodology to determine the strain distribution within the binder domains. Elastic properties for the binder and the aggregate phases were used in this study and the average strain in the binder phase was shown to be an average of 7.8 and a maximum of 510 times the bulk strain of the asphalt mixture [29]. It was also shown that the strain within the binder phase decreased if air voids were considered in the analysis. Many studies have focused on the micromechanical analysis of hot mix asphalt (HMA), but a clear consensus on the distribution of stress and strain in the binder phase of HMA is lacking.

In the present chapter finite-element analysis and image analysis methods were used to simulate the behavior of asphalt mixtures and study the effect of the binder properties and aggregate gradation on their rutting performance. The aggregate gradations and the binders used in this study were mentioned in the previous chapter (Figure 3-5, Figure 3-7, and Figure 3-8).

5.1 Mastic Scale

Four different volume fractions (φ), 0.1, 0.2, 0.3 and 0.4, were used to study the stress and strain distribution in matrix of mastic scale. To determine the optimum RAE, four mastic areas were

modeled and analyzed, using a filler volume fraction of 0.4, as the largest and most critical volume fraction considered in this study. The largest area was selected as 750 µm × 750 µm, 10 times larger than the maximum filler particle size. Three smaller subset areas (450 µm × 450 µm, 225 µm × 225 µm and 150 µm × 150 µm) were also obtained from the original image for RAE analysis, as shown in Figure 5-1. Finite element analysis was used to obtain the creep compliance curve for each image through bulk strain measurement under uniform compressive loading.

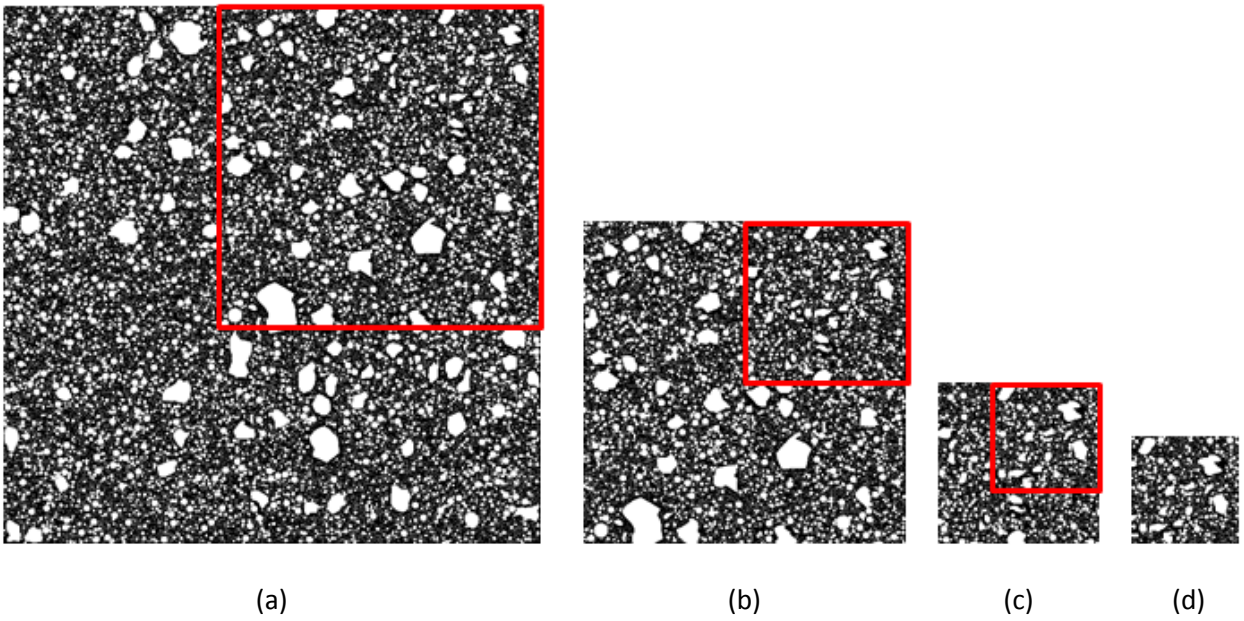

Figure 5-1: Image analysis procedure to find optimum RAE size of the GS mastic. (a) 750 µm × 750 µm (b) 450 µm × 450 µm (c) 225 µm × 225 µm (d) 150 µm × 150 µm

The optimum RAE size was selected based on the convergence of the measured gradation and creep compliance curves of each of the modeled mastic areas to that of the original large scale image. Results for the GS mastic are shown in Figure 5-2 and Figure 5-3. Figure 5-2 shows that as the size of the RAE increased the observed gradation curves quickly converged to the inputted gradation of the original image. Similar trends were observed for the creep compliance

in Figure 5-3, showing a sharp divergence form the original image for the 150 µm × 150 µm image. The optimum RAE size for all three filler types was determined to be a 225 µm × 225 µm area, which was used for all subsequent analysis at the mastic scale.

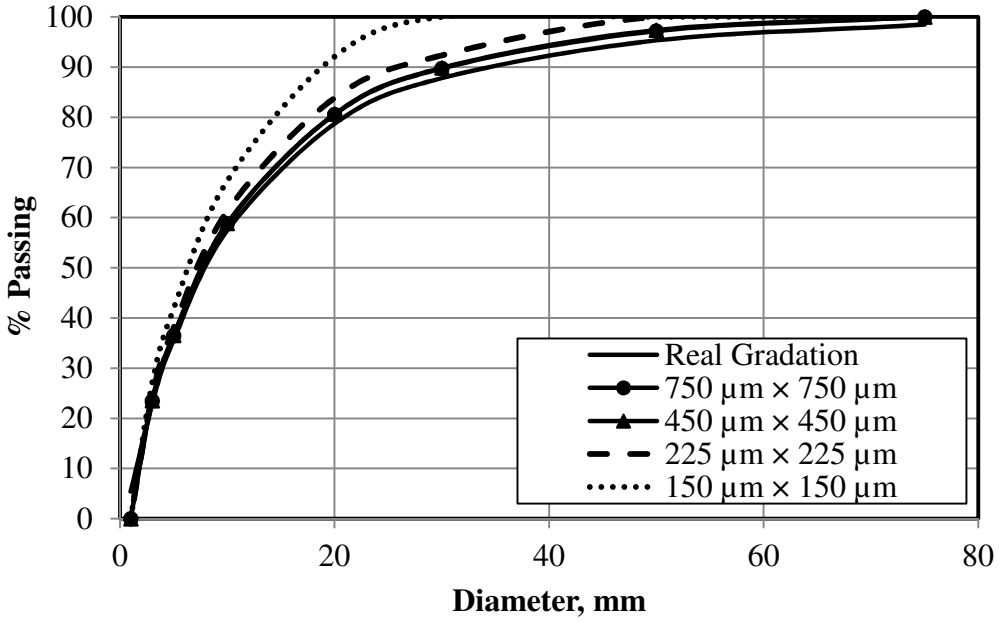

Figure 5-2: Gradation of the generated GS mastic images

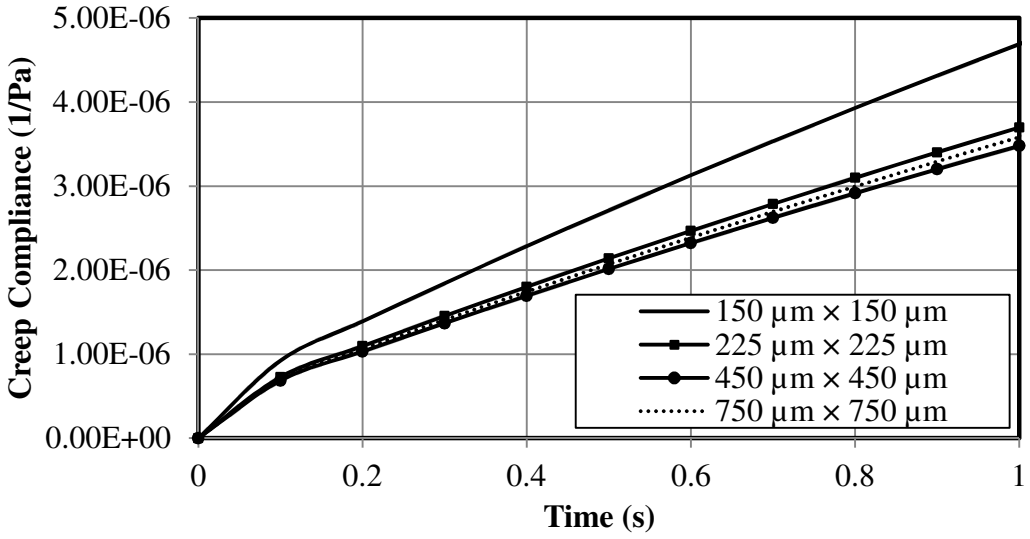

Figure 5-3: Creep Compliance of the generated GS mastic images

Using the determined optimum RAE and varying the volume fractions between 0.1, 0.2, 0.3 and 0.4, mastic scale models were generated for each filler gradation and binder properties. These mastics were placed under creep loading and the stress distribution in the binder phase of each was derived at the end of the loading cycle (1 second) through a finite element simulation process.

For assessment of the stress level in the continuous matrix of the mastic scale, stress-per-element histograms were plotted against normalized element frequency (Figure 5-4). Figure 5-4 shows that as the volume fraction of the filler increases in the mastic, the bell shaped curve of the stress histogram changed from a tall and narrow curve to a broad and flat one. Furthermore, by increasing the filler volume fraction, the overall stress decreased in the binder matrix. At lower volume fractions the level of stress in the binder phase was found to be similar to the stress applied to the mastic model; in other words, in the absence of an effective load bearing filler network at low volume fractions, the binder phase transfers most of the applied load at the mastic level. In the case of $\varphi=0$, the minor (most compressive) principal stress in all binder elements is equal to the applied compressive stress; therefore the stress-per-element histogram curve would be a Dirac delta function shifted horizontally to the value of the applied stress.

As was mentioned in chapter 3, in the first binder group, four different binders with different levels of instantaneous elastic and delayed elastic responses were used in this study: (1) High Instantaneous elastic response and High Delayed elastic response (HIHD), (2) High Instantaneous elastic response and Low Delayed elastic response (HILD), (3) Low Instantaneous elastic response and High Delayed elastic response (LIHD), and (4) Low Instantaneous elastic response and Low Delayed elastic response (LILD) (Figure 3-7).

To facilitate discussion and comparison, the ratio of the average of maximum compressive stress in all continuous phase elements to the total normal stress applied to the model at that scale, is defined as "α". As the overall trend in all mastic types (three different filler gradations and four different binders) was similar, the analysis in this section will be primarily focused on the GS mastic with HIHD binder, with overall comparisons of all three mastic types presented at the end. For the GS mastic the value of α for filler volume fractions of 0.1, 0.2, 0.3 and 0.4 was 0.94, 0.90, 0.83, and 0.72, respectively.

At lower volume fractions the distance between the filler particles is larger than the particle size; in such conditions the filler is effectively "diluted" in the viscoelastic binder matrix (Yin et al, 2008). Particle interactions are considered to be negligible in diluted blends. By increasing the volume fraction, particles proximity increases, and particle interaction increases as particle networks gradually form in the mastic. As the particle networks expands at higher volume fractions, the load transfer efficiency of the network increases, thus transferring a larger portion of the mastic load, effectively decreasing stress levels in the binder matrix. Repeating this analysis for shear stress in the binder phase yielded a similar trend as that of the minor principal stress, with α decreasing from 0.43 at φ=0.1 to 0.21 at a φ=0.4 volume fraction.

Figure 5-5 further highlights the above discussion through the demonstration of Von-Mises stress contours in the GS mastic at different volume fractions. The stress contours clearly show that the stress in the binder matrix decreased as the filler volume fraction increased in the mastic. Furthermore, stress in the binder phase is observed to be mainly concentrated at the binder-filler interface, especially where the filler particles are in close proximity of each other, forming particle to particle contact points.

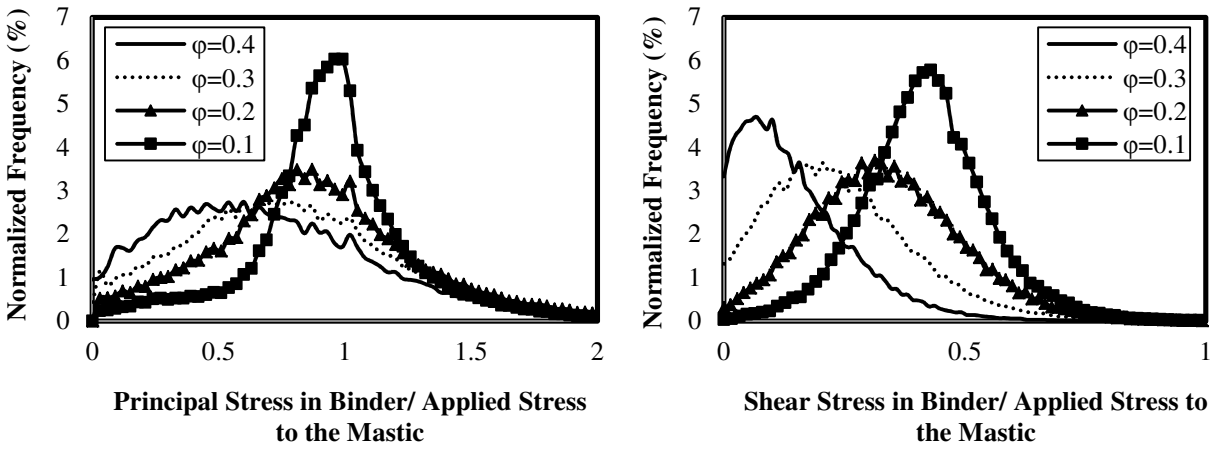

Figure 5-4: Histograms of principal and shear stress in binder phase of GS mastic with HIHD binder (ϕ is filler concentration by volume in mastic)

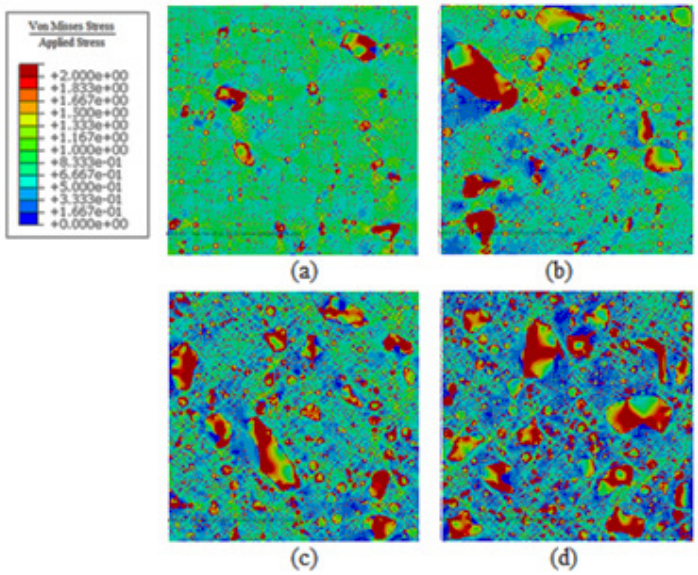

Figure 5-5: Contour of Von Mises stress in GS mastics (a) ϕ=0.1 (b) ϕ=0.2 (c) ϕ=0.3 (d) ϕ=0.4

The minor principal stress histograms for the three considered filler types at a constant volume fraction of 0.3 are plotted in Figure 5-6. As shown, the finer gradations of the GS and LS fillers resulted in reducing the stress in the binder matrix compared to the DS fillers due to the considerably higher specific area for the later filler type. The stress ratio α for the GS, LS, and

DS mastics at 0.3 volume fraction was calculated as being 0.73, 0.74 and 0.80, respectively. As previously shown in Figure 3-12, GS and LS mastics have similar gradations; as a result the stress levels in these two mastics are not much different.

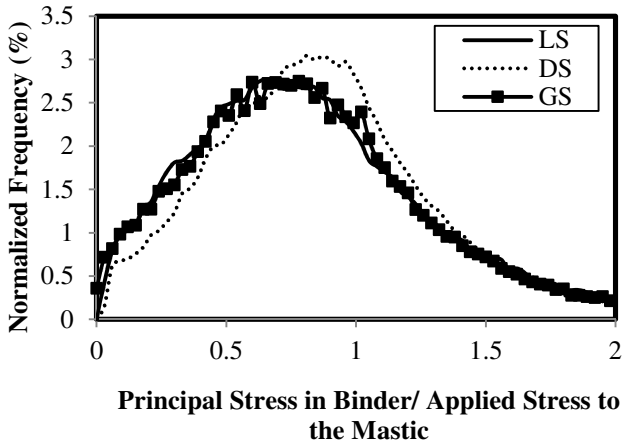

Figure 5-6: Histogram of principal stress in binder phase of GS, LS and MS mastic at ϕ=0.3

The minor principal stress histograms of binder phase of GS mastics of four different binders of first binder group, defined in chapter 3, show that by increasing the volume fraction of the fines in the mastic the continuous matrix elastic component effect on stress distribution in the matrix increases (Figure 5-7). It should be noted that although all of the binders studied in the first group of binders have same viscous component, their elastic component are different. Figure 3-7 shows that HIHD binder has the lowest and LILD binder has the highest stiffness among these binders. It was mentioned earlier that most of the applied stress to the scale transfers through the particle networks. It means that the effect of continuous matrix on bulk strain of the scale decreases by increasing the particle volume fraction or initiation of particle networks. In the case of no interaction between the particles, the stress applied to the scale transfers directly to the matrix; therefore, the stress level of matrix is not a function of its elasticity as shown in Figure 5-7. Figure 5-7 highlights the above discussion using binder phase

principal stress histograms for four different binders. It can be seen that HIHD binder which has the highest elastic response has the lowest stress as well.

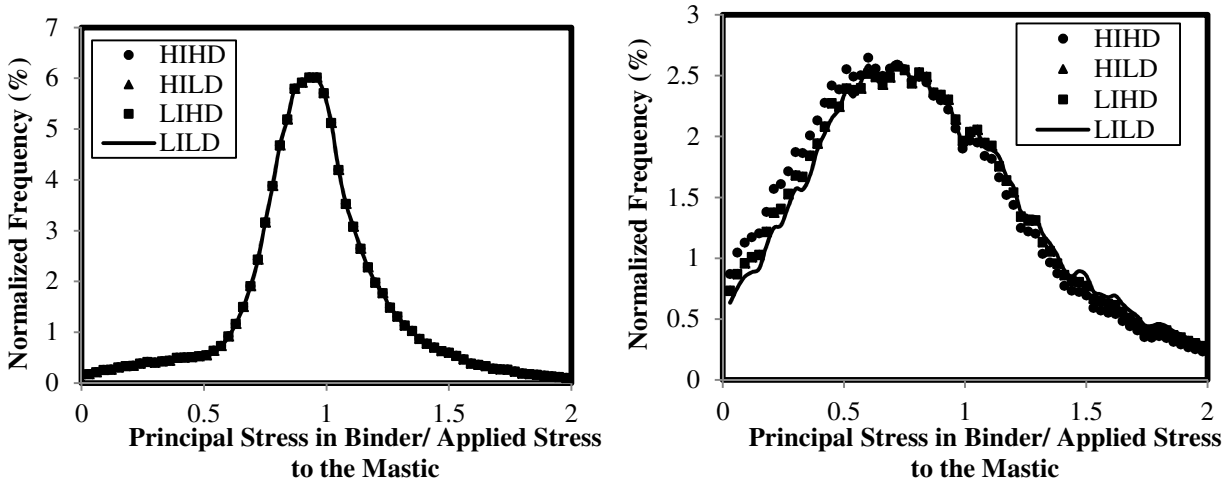

(a) φ=0.1 (b) φ=0.4

Figure 5-7: Histogram of principal stress in GS mastic: (a) ϕ=0.1 (b) ϕ=0.4

The strain distribution in the mastic phase was also analyzed in the present study. Analysis on GS mastic with HIHD binder showed that the average shear strain in the binder at 0.1, 0.2, 0.3 and 0.4 volume fractions were respectively 1.11, 1.30, 1.58 and 2.04 times the mastic's bulk strain. Analysis showed that the binder effect on mastic's bulk strain decreased significantly at φ=0.4, due to the initiation of particle interaction in the mastic. Figure 5-8 illustrates the state of strain in the binder phase through the use of minor principal strain histograms at different volume fractions. To allow for the determination of the effect of the mineral filler on the mastic scale strain field, the strain values in Figure 5-8 are normalized to the strain of a pure binder model with no filler particles in the matrix. For filler volume fractions of 0.1, 0.2 and 0.3 the bell shaped strain histogram become broader and flatter as the volume fraction increased, with the peak moving toward lower average strain values. However, the trend changed significantly upon reaching a 0.4 volume fraction. This was attributed to the

considerable increase in zero-strain binder elements at 0.4 volume fraction due to formation of an effective particle-to-particle network in the mastic.

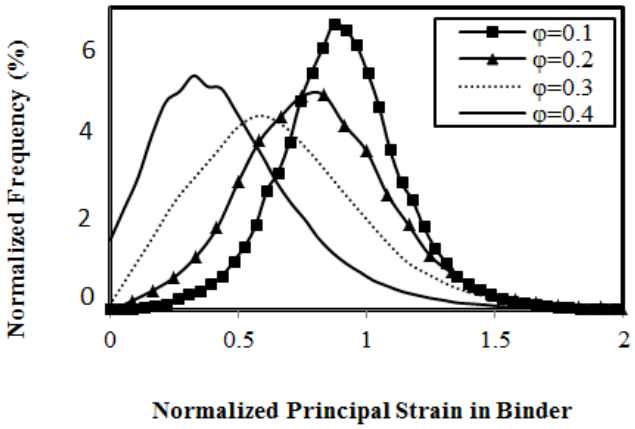

Figure 5-8: Histogram of minor principal (maximum compressive) strain in binder phase of GS mastic

Similar stress and strain analysis performed on the mastic scales of the binders of the second binder group. The minor principal stress histograms of binder phase of GS mastics of four different binders of second binder group, defined in third chapter, show that by initiation of particle interaction in the mastic the continuous matrix properties effect on stress distribution in the matrix increases Figure 5-9.

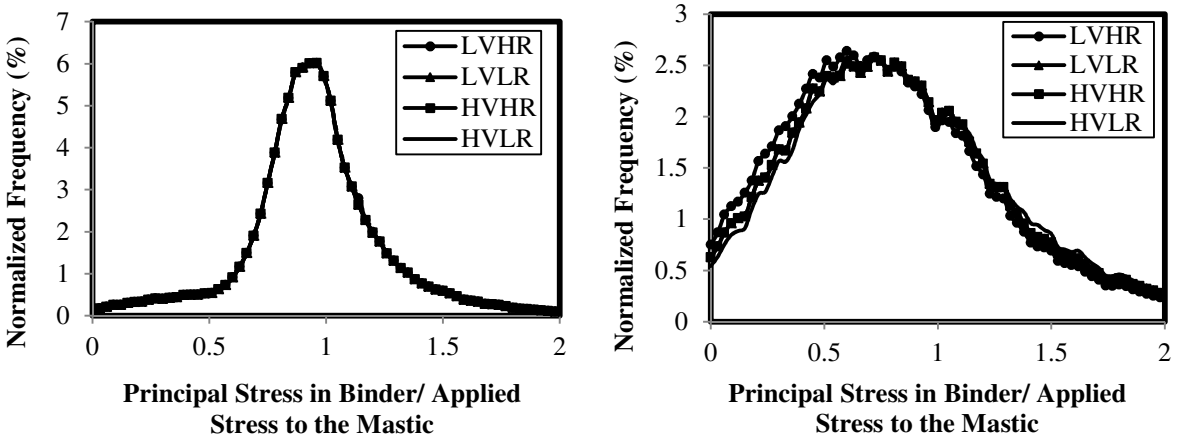

(a) φ=0.1 (b) φ=0.4

Figure 5-9: Histogram of principal stress in GS mastic: (a) ϕ=0.1 (b) ϕ=0.4

5.2 Mortar Scale

For determination of the input properties for the mortar scale of the multi-scale model, the viscoelastic properties of the mastic scale assessed by performing a creep and recovery simulation on the mastic RAE, and fitting the Burger's model to the analysis results. The appropriate filler volume fraction was determined from the aggregate gradation curve, while the laser diffraction derived gradation for particles passing #200, shown in Figure 3-12 were applied to the model. The Burger's model parameters were converted to Prony series parameters through the use of the methodology explained in equations (1) through (7) in chapter 3. These properties were used as material input values for the continuous matrix of mortar scale of the multi-scale simulations. Mastic was assumed to be isotropic and homogenous in the mortar scale.

The volume fraction of fine aggregates in mortar scale was determined based on the mix gradation and mix design properties. It was calculated that for regular asphalt mixture designs the volume fraction of the fine aggregates in mortar scale varies from 0.4 to 0.55. In comparison, the volume fraction of fillers in the mastic scale ranged from 0.1 to 0.4. Coarser overall mixture aggregate gradations result in lower volume fraction of fines in the mortar and mastic scales. Based on convergence of the creep compliance curves and fine aggregate gradations, an optimum RAE of 3.5 mm × 3.5 mm, approximately 3 times larger than the maximum size of fine aggregates in mortar scale was determined. Similar to the property input from the mastic to the mortar scale, material properties from the mortar scale were identified by performing a creep and recovery simulation on the mortar RAE, fitting the Burger's model, and converting to Prony series parameters. Results are inputted as material properties in the continuous matrix of the "asphalt mixture scale", assuming an isotropic and homogeneous mortar matrix at this scale.

5.3 Asphalt Mixture Scale

As previously discussed, three distinct aggregate gradation types were used in the study of the asphalt scale mixtures. Aggregate volume fraction in the coarse, intermediate and fine graded mixtures was respectively 0.65, 0.58 and 0.49, with finer gradation having the lower volume fractions (Table 3-1). It must be noted that the total aggregate volume fraction were similar for all samples.

Figure 5-10 shows results of the RAE determination analysis for the asphalt scale. The aggregate volume fraction was determined for progressively smaller portions of the original images, and the aggregate volume fraction in each image was determined and compared to that of the original image. It can be seen that the volume fraction measurements began to diverge from the actual value when the sampling area was decreased under 16 cm^2. Similar results were found for analysis based on the convergence of aggregate gradation and creep compliance curves for the images, resulting in the selection of an optimum RAE of 40 mm × 40 mm for the asphalt scale.

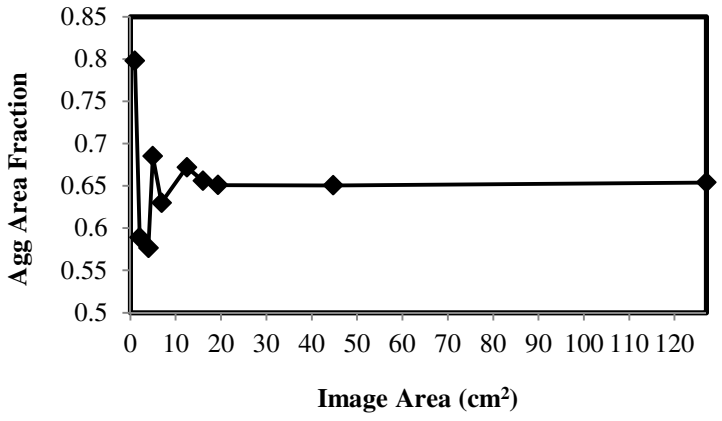

Figure 5-10: Aggregate volume fraction of RAEs

To assess the shear stress distribution in the binder phase, it was necessary to transfer the average of minor principal stress components in the continuous phase elements of each higher scale to the next lower scale. The minor principal stress is the maximum compressive stress that each element experiences. The average of minor principal stresses in the mortar phase at the asphalt scale is applied as a compressive load to the mortar scale model. Similarly, in turn the average of minor principal stresses in the mastic phase model was then determined and applied as a compressive stress to the mastic scale, and consequently the shear stress distribution in the binder phase is then determined under the scale by scale transfer of compressive loads from the asphalt scale down to the binder scale.

Minor principal stress histograms for the mortar scale continuous phase (the mastic scale with HIHD binder) are plotted for all three gradations in Figure 5-11. The ratio α for the mortar scale of the fine, intermediate and coarse graded mixtures was found to be 0.30, 0.41 and 0.57, respectively. Due to higher volume fraction in the mortar phase of the finer gradation mixtures, the mastic stress levels in the fine gradation mixture was found to be lower than that of the intermediate and coarse mixtures. The intermediate and coarse graded mixtures have less fines and consequently lower volume fractions in their mortar and mastic scales, leading to higher load transfer to the binder phase for these gradations. Distribution of the particles in the matrix for the scales that the particle volume fraction is high such that there is an effective aggregate skeleton, the major portion of the applied stress is carried by the particle skeleton and the matrix elements in the vicinity of the skeleton. A minimal portion of applied stress is carried by other matrix elements which are not in the vicinity of the skeleton; however, there is a bell shaped stress distribution for the matrix elements at the vicinity of the skeleton. Therefore, the whole stress distribution in the matrix phase is a combination of a bell shaped stress distribution for matrix

elements around the particles and a stress distribution with high number of minimal (i.e. close to zero) stress level elements which explains the two peaks in the stress distribution curves (Figure 5-11).

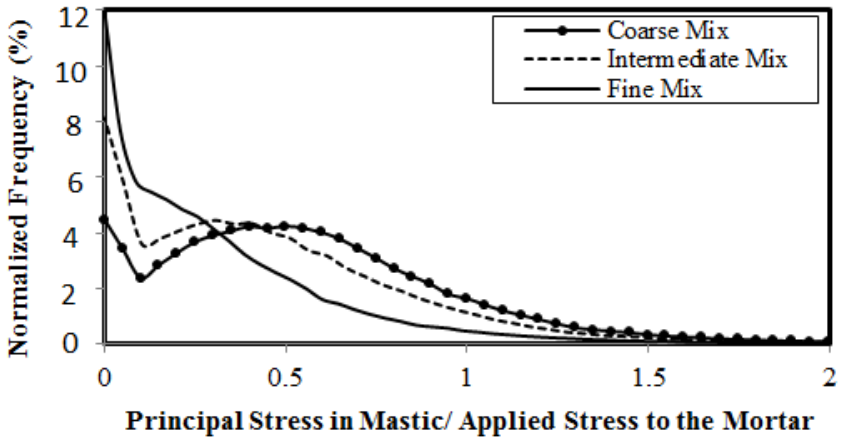

Figure 5-11: Histogram of principal stress in mastic phase of mortar of fine, intermediate and coarse mixes

Minor principal stress histograms of mastic phase of fine mixture are plotted for all of the first group binders in Figure 5-12. As it can be seen like binder phase, as the mastic phase is more elastic its stress level is lower. It is obtained that the ratio α for the HIHD, LIHD, HILD, and LILD mastics are 0.3, 0.33, 0.33, and 0.36, respectively. Thus among the binders with the same viscous component the one with higher elastic component decreases the stress level in the mastic phase as well as the binder phase.

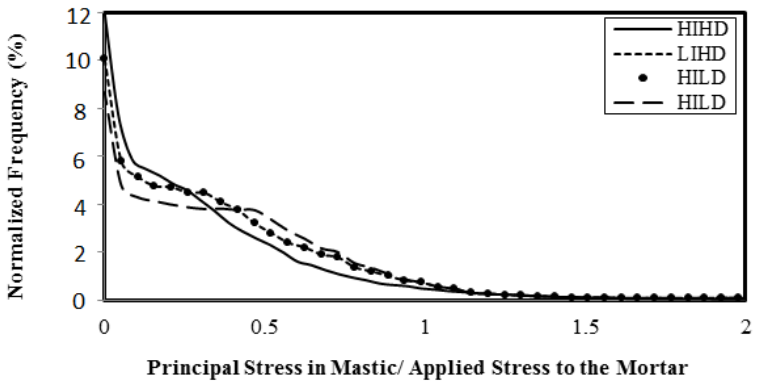

Figure 5-12: Histogram of principal stress in continuous phase of mortar of fine mixture

Similar analysis was performed to assess minor principal (maximum compressive) stress levels in the mortar phase of the asphalt mixtures (Figure 5-13). From Table 3-1 it can be seen that as the volume fraction of aggregates increases in the asphalt scale, the volume fraction of fine aggregates in the mortar scale decreased, consequently softening the matrix. Therefore, it is expected that the mortar matrix in the coarse graded mixture to have lower stress levels due to its softer mortar matrix and its higher volume fraction of aggregates. Results from the FE analysis of the asphalt scale confirm this expectation, as the α values decreased as the gradation became coarser, with α values for the fine, intermediate and coarse graded mixtures being 0.51, 0.25 and 0.22, respectively.

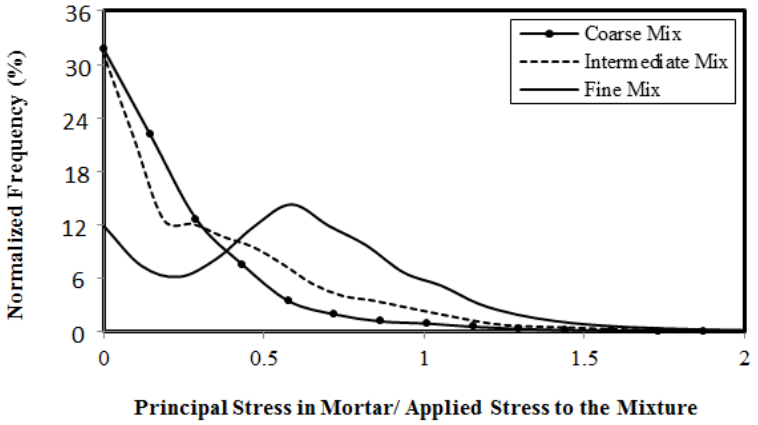

Figure 5-13: Histogram of principal stress in mortar phase of fine, intermediate and coarse mixes

A same analysis was performed on the HIHD, LIHD, HILD, and LILD mortars of fine gradation mixture. Figure 5-14 shows the minor principal stress histograms of the mortar phases. The α value was determined for the mortars to be 0.51, 0.53, 0.53, and 0.55 for HIHD, LIHD, HILD, and LILD mortars, respectively. The same analysis for binders of the second group showed that the mortar of LVHR experiences the lowest stress during its loading time (Figure 5-15).

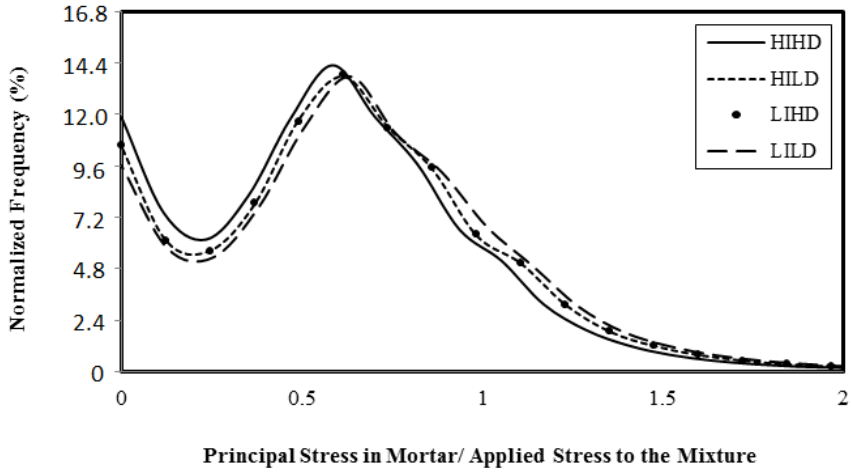

Figure 5-14: Histogram of principal stress in continuous phase of asphalt mixture scale of fine mixture (First Binder Group)

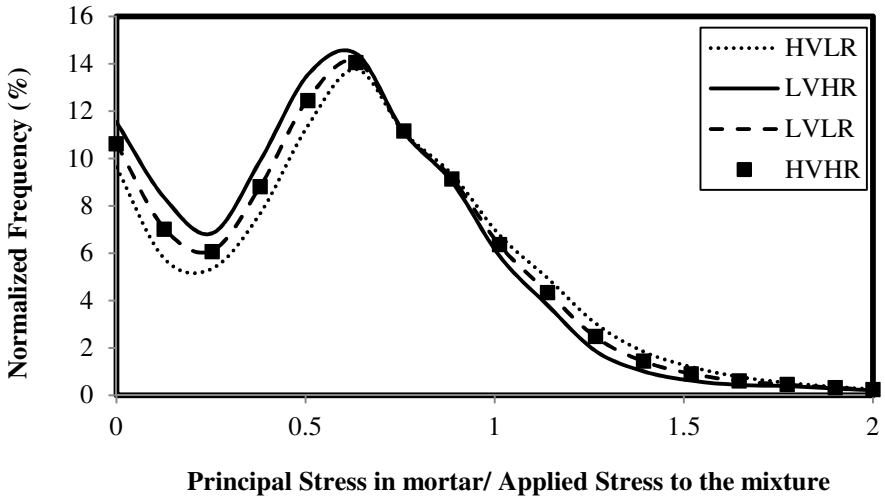

Figure 5-15: Histogram of principal stress in continuous phase of asphalt mixture scale of fine mixture (Second Binder Group)

Extending the analysis results to the case of a standard 18 kip (80 kN) load, the average shear stress in the binder phase of all of the mixtures considered in this study were calculated (Table 5-1). It was also determined that among the binders which have same viscous component the one with higher elastic response shows lower stress level in the binder phase of mixture due to its lower stiffness during the loading time. In another word if the binders have same viscous component the one with higher elastic component will force more stress to be carried by the aggregates. Since aggregates are perfectly elastic, that increase in stress in aggregates will not cause more permanent deformation. However lower stress in binder phase will result in lower permanent deformation of total mixture.

Table 5-1: Average shear stress level (KPa) in binder phase of mixtures with binders of first group

Binder \ Gradation	Fine	Intermediate	Coarse
HIHD	14	11	22
LIHD	16	12	23
HILD	16	12	23
LILD	18	13	24

Figure 5-16 shows the permanent deformation of the mixtures after 50 cycles of loading. As can be seen, the mixture with HIHD binder shows the lowest permanent deformation while the mixture with LILD binder shows the highest permanent deformation. The results also show that the LIHD and HILD binders, which have same elastic response but different instantaneous elastic and delayed elastic response, affect the rut resistance of asphalt mixture similarly. Among the binders with same viscous component, the one with higher elasticity leads to lower deformation in asphalt mixture as well as lower stress in asphalt binder phase. It should be noted that although these binders show same permanent deformation at the end of the recovery when

tested alone, their corresponding mixtures show different permanent deformation due to the differences between the binder stiffness during the loading time. As shown in Table 5-1 the binder with higher elastic strain response is softer and thus leads to lower stress in the mixture as more stress is taken by the aggregates. This lower stress leads to lower permanent deformation of the mixture as final permanent strain is proportional to stress with binder.

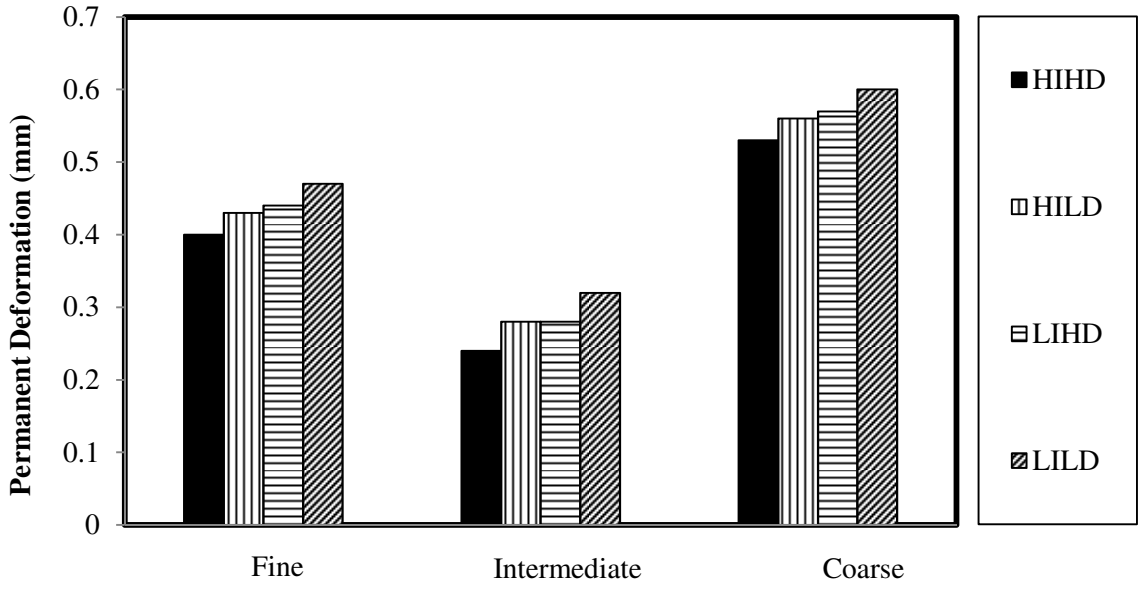

Figure 5-16: Permanent Deformation of the mixtures after 50 cycles of loading

It is interesting to note that for all of the gradations, mixtures containing LIHD and HILD binder show the same average shear stress in their binder phase and almost the same permanent deformation after 50 cycles of loading. Furthermore for all of the gradations the mixtures containing LILD binder has higher stress level in binder phase than the mixtures containing HIHD binder and the difference between their permanent deformations after 50 cycles of loading is almost the same for all three aggregate gradations. Figure 5-17 highlights the above discussion on the effect of stress level in the binder phase on permanent deformation of the

mixture by making a comparison between the permanent deformation of the LILD and HIHD binders under the same stress as they experience in their corresponding mixtures with fine aggregate gradation (18 kPa for the LILD and 14kPa for the HIHD).

Figure 5-18 shows the stress level in the binder phase of the mixtures studied in fourth chapter at the initial, primary, and secondary stages.

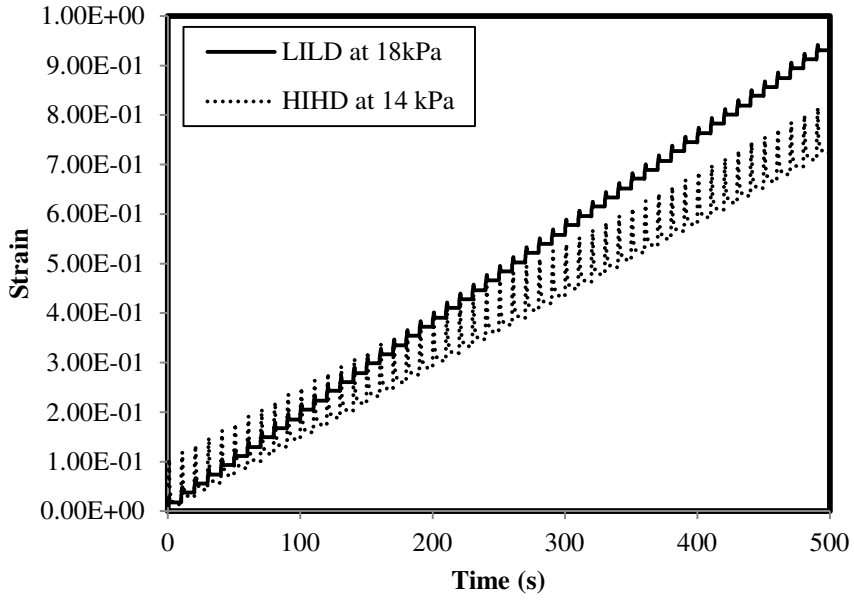

Figure 5-17: Comparison between the permanent deformation of the LILD and HIHD binders under the stress level experienced in the corresponding fine graded mixture

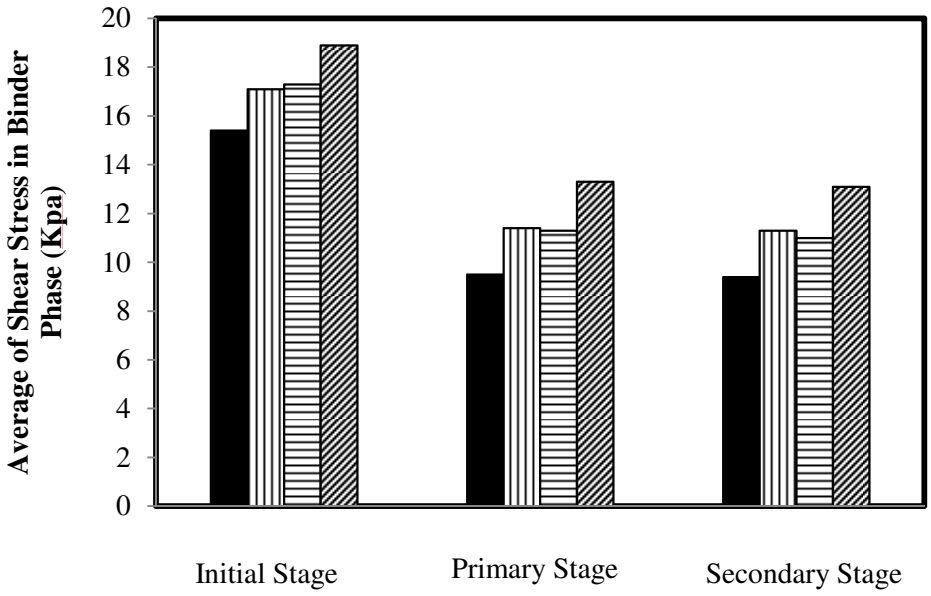

Figure 5-18: Average shear stress level (KPa) in binder phase at different stages of rutting

As was previously mentioned in third chapter, the second group of binders in this study includes for binders with two levels of viscous component and two levels of elasticity in order to compare binder elasticity and viscosity effects on rut resistance of asphalt mixtures: (1) High Viscous component binder with Low Recovery (HVLR), (2) Low Viscous component binder with Low Recovery (LVLR), (3) High Viscous component binder with High Recovery (HVHR), and (4) Low Viscous component binder with Low Recovery (LVLR) (Figure 3-8). Table 5-2 shows the stress level in binder phase of the fine, intermediate, and coarse graded mixtures with the binders of the second group. It can be concluded that lower viscous component binder as well as the binder with higher elasticity leads to lower shear stress in the binder phase of the asphalt mixtures.

Table 5-2: Average shear stress level (KPa) in binder phase of mixtures with binders of second group

Gradation / Binder	Fine	Intermediate	Coarse
HVLR	18	13	24
LVLR	16	12	23
HVHR	16	12	23
LVHR	15	11	22

Although the stress level is lower during the loading time in the case of the binder with lower viscous component (higher permanent deformation under the same loading), the permanent deformation in asphalt mixture with HVLR is much lower than the permanent deformation of the mixture with LVHR (Figure 5-19). Figure 5-19 shows the permanent deformation in the mixtures after 50 cycles of loading.

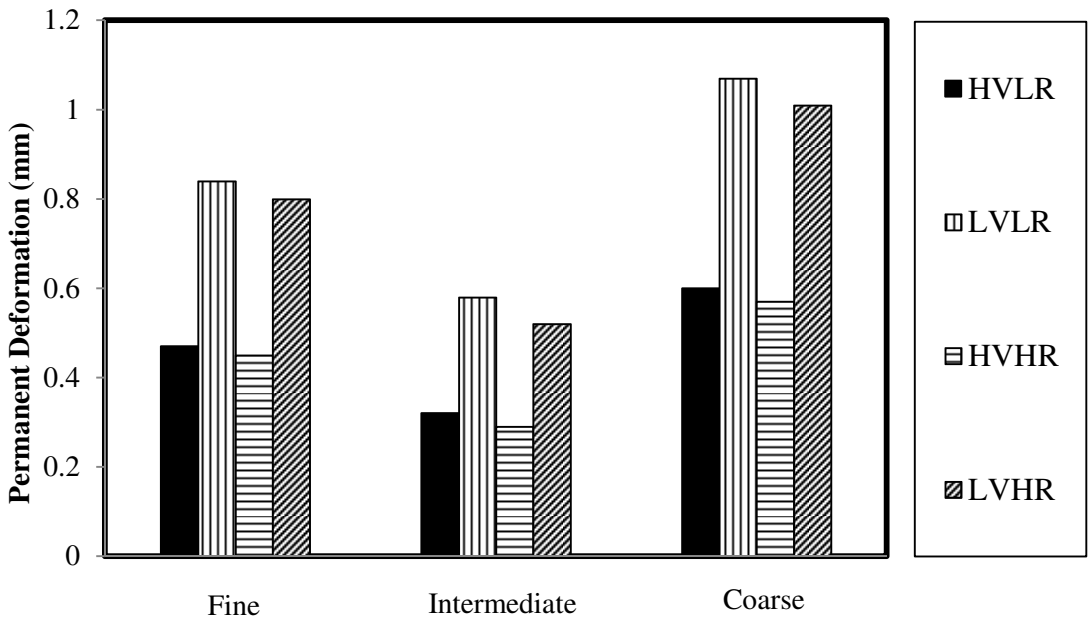

Figure 5-19: Permanent Deformation of the mixtures after 50 cycles of loading

It can be concluded that although the mixture containing the binder with higher stress level has the higher permanent deformation in the case of binders with same viscous component

(permanent deformation); among the binders with different viscous components this statement is not valid.

6. Practical Applications

This study developed a multi-scale model of asphalt mixture containing the three main phases of asphalt pavements, binder, aggregate, and air voids. This model and the analysis performed yields three main practical applications:

1. Recommending an optimum type of binder modification to maximize mixture rutting resistance.
2. Determination of applicable experimental stress levels to be used for rutting performance characterization tests for asphalt binders (e.g. the MSCR test), such as to realistically represent actual conditions within the asphalt pavements.
3. Determination of the effect of aggregate gradation on the mixture stress and strain distribution, thus providing a quantitative basis for choosing the optimum gradation to enhance rutting resistance.

6.1. Optimum Modification Type for Rutting Resistance

Based on the results it can be concluded that the permanent deformation of the mixtures containing binders with higher viscous component (lower permanent deformation) is lower. It was also found that for the binders which have the same viscosity level (the same permanent deformation under the same step stress), the permanent deformation and the binder stress level in the mixtures containing binders with higher instantaneous and delayed elasticity are lower than the low elasticity ones; however the effect of elasticity on rutting is minor in comparison with the effect of asphalt binder viscosity. Therefore, polymer modifiers that limit binder permanent deformation will improve rutting resistance of asphalt mixture much more than the modifiers which make the binder more elastic based on the results of this study.

6.2. Optimum Aggregate Gradation for Rutting Resistance

Three different aggregate gradations were used in this study. Higher volume fraction of aggregates and filler are shown to lead to a decrease in stress in the continuous phase of each scale, and ultimately in the binder phase. This is believed to be due to the increase in particle proximity and interaction at high volume fractions, leading to the formation of load-transferring structural networks. Such networks redistribute stresses through the particle network, effectively leading to an overall reduction in stress levels in the continuous phase of each scale. Therefore it can be helpful to increase the filler volume fraction in coarse graded mixtures to decrease the stress and strain level of the asphalt mixture.

Overall it was shown that a well graded intermediate gradation (between coarse and fine limits across all sieve sizes) will minimize the stress level in the binder phase and maximize load transfer by the aggregate structure. Furthermore it is recommended that filler content (P200) be higher than approximately 5% by weight of aggregate.

6.3. Recommended Binder Stress Levels for Binder Rutting Characterization Tests

The stress levels in binder of the mixtures studied in this thesis are much greater than the 3.2 kPa stress level applied to binder samples used in the Multiple-Stress Creep and Recovery (MSCR) (AASHTO T-70, 2009) test for assessment of binder rutting resistance. Such results may indicate the need to consider an additional higher stress level in the MSCR test procedure to better represent binder stress state in the mixture.

7. Conclusions and Summary of Findings

In the present study a multi-scale analysis utilizing finite-element methodology and image analysis was developed to simulate the binder elasticity and binder viscosity effects on rut resistance of asphalt mixture. The results of this dissertation prove the hypothesis that binder elasticity and binder viscosity affect the rut resistance of hot mix asphalt. It was concluded that polymer modifiers that limit binder permanent deformation will improve rutting resistance of asphalt mixture much more than the modifiers which make the binder more elastic.

In the case of aggregate gradation it was shown that a well-graded, intermediate gradation is capable of generating effective particle skeleton in micro- and macro-scale, thus reducing binder stress levels over all scales of the asphalt mixture. Overly fine aggregate gradation could prevent effective formation of aggregate networks at the macro scale. On the other hand use of overly coarse gradations leads to lower volume fractions at the micro scale, impeding network formations at that scale, leading to softer mastic and mortar matrixes.

A realistic material model should take into account the evolution of the microstructure during the rutting process in asphalt mixture. The limitations of the FE approaches used to simulate the asphalt mixture behavior are the inability to model changes in the aggregate contact geometry and capturing the aggregates coming into contact or out of contact.

8. Recommendations for Future Work

The FE analysis conducted in this study is based on the elements with same sizes and shapes. It is recommended that future work focus on the generation of a smart meshing procedure, as well as introduces subroutines for defining aggregate movement and friction on one another and aggregate damage to increase the accuracy of the model in simulation the behavior of asphalt mixture. It is anticipated that such measures will enable the models to the asphalt mixture behavior in the tertiary zone of rutting.

Working on expending the used finite element analysis in this study from 2D to three dimensional microstructures is recommended.

9. Bibliography

[1] J. B. Sousa, J. A. Deacon, S. L. Weissman, R. B. Leahy, J. T. Harvey, G. Paulsen, J. S. Coplantz and C. L. Monismith, "Permanent Deformation Response of Asphalt Aggregate Mixes," Strategic Highway Research Program, National Research Council, Washington D. C., 1994.

[2] S. L. Weissman, J. T. Harvey, J. L. Sackman and F. Long, "Selection of Laboratory Test Specimen Dimension for Permanent Deformation of Asphalt Concrete Pavements," *Transportation Research Record 1681, Transportation Research Boards,* pp. 113-120, 1999.

[3] S. L. Weissman, "The Mechanics of Permanent Deformation in Asphalt Aggregate Mixtures: A Guide to Laboratory Test Selection," *Symplistic Engineering Corp,* p. 55, 1997.

[4] J. A. Scherocman, "Guidelines for Compacting Asphalt Concrete Pavement," *Better Roads,* vol. 54, no. 3, pp. 12-17.

[5] M. D. Beer, L. Kannemeyer and C. Fisher, "Towards Improved Mechanistic Design of Thin Asphaltic Layer surfacing based on Actual Type/Pavement Contact stress - In - Motion (SIM) Data in South Africa," in *7th Conference on Asphalt Pavements for Southern Africa*, 1997.

[6] H. U. Bahia, D. I. Hanson, M. Zeng, H. Zhai, M. A. Khatri and R. M. Anderson, "Characterization of Modified Asphalt Binders in Superpave Mix Design," NCHRP Report 459, TRB, National Research Council, Washington, D.C., 2001.

[7] H. U. Bahia, "Critical Evaluation of Asphalt Modification Using the SHRP Concepts," *Transportation Research Record 1488,* pp. 82-88, 1995.

[8] R. L. Terrel and I. A. Epps, "Using Additives and Modifiers in Hot Mix Asphalt," *QI Series 114, National Asphalt Pavement Association (NAPA),* 1989.

[9] G. D. Airey, "Rheological Properties of Styrene Butadiene Styrene Polymer Modified Road Bitumens," *In Fuel,* vol. 82, pp. 1709-1719, 2003.

[10] U. Isacsson and X. Lu, "Properties of bitumens modified with elastomers and plastomers," in *2nd Euroasphalt & Eurobitumen Congress*, Barcelona, 2000.

[11] Y. Yildirim, "Polymer Modified Asphalt Binders," *Construction and Building Materials,* vol. 21, no. 1, pp. 66-72, 2007.

[12] King, Gayle, Helen King, R. D. Pavlovich and L. E. Amy, ".Additives in Asphalt," *Association of Asphalt Paving Technologists,* vol. 68A, 1999.

[13] B. Brule, "Polymer-Modified Asphalt Cements Used in the Road Construction Industry: Basic Principles," *Transportation Research Record 1535,* p. 48–53, 2007.

[14] S. Tayfur, H. Ozen and A. Aksoy, "Investigation of rutting performance of asphalt mixtures containing polymer modifiers," *Construction and Building Materials,* pp. 328-337, 2005.

[15] N. Roohi, L. Tashman and H. U. Bahia, "Internal Structure Characterization of Asphalt Mixtures for Rutting Performance Using Imaging Analysis," *Road Materials and Pavement Design,* vol. 13, pp. 21-37, 2012.

[16] A. Hofstra and A. J. G. Klopm, "permanent deformation of flexible pavements under simulated road traffic conditions," *Transportation Research Record 1681, Transportation Research Boards,* pp. 613-621, 1972.

[17] J. Eisenmann and A. Hilmer, "Influence of Wheel Load and Inflation Pressure on the Rutting Effect at Asphalt-Pavements - Experiments and Theoretical Investigations," in *Proceedings, Sixth international Conference on the Structural Design of Asph*, 1987.

[18] P. Uge and P. Van de Loo, "Permanent Deformation of Asphalt Mixes," in *Koninklijke/Shell-Laboratorium*, Amsterdam, 1974.

[19] K. Mahboub and D. N. Little, "Improved Asphalt Concrete Design Procedure," Research Report 474-1F, Texas Transportation Institute, 1988.

[20] C. Monismith, J. Epps and F. N. Finn, "Improved Asphalt Mix Design," *Association of Asphalt Paving Technologists,* vol. 54, pp. 347-406, 1985.

[21] S. F. Brown and C. L. Bell, "The Validity of Design Procedures for the Permanent Deformation of Asphalt Pavements", Proceedings, Fourth International Conference on tire Structural Design of Asphalt Pavements," Ann Arbor, 1997.

[22] "Large stone mixes: A historical insight," Maryland, 1988.

[23] A. F. Faheem, H. U. Bahia and H. Ajideh, "Estimating results of a proposed simple performance test for hot-mix asphalt from superpave gyratory compactor results," *Transportation Research Record 1929,* p. 104–113, 2005.

[24] J. Kim, H. L. Moseley and G. A. Sholar, "Investigation of Shear Failure of HMA Using Rotary Asphalt Wheel Tester (RAWT)".

[25] F. Zhou and T. Scullion, "Model Calibrations with Local Accelerated Pavement Test Data and Implementation for Focused on Solution to NAFTA Problems," Texas Transportation Institute at Texas A&M University, College Station, 2002.

[26] H. Ying, "X-ray computed tomography to quantify damage of hot-mix asphalt in the dynamic complex modulus and flow number tests," MSc thesis. Louisiana State University, 2010.

[27] O. C. Zienkiewicz and R. L. Taylor, The Finite Element Method, 4 ed., vol. I, McGraw-Hill International (UK) Limited, 1988.

[28] J. N. Reddy, An Introduction to the Finite Element Methodthe second edition, McGraw-Hill, Inc, 1993.

[29] S. Kose, M. Guler, H. U. Bahia and E. Masad, "Distribution of strains within asphalt binders in HMA Using Image and finite element techniques," *Trans Res Record National Research Council,* 2000.

[30] K. Sepehr, O. J. Harvey, Z. Q. Yue and H. M. El Husswin, "Finite element modeling of asphalt concrete microstructure," in *3rd Int Conf Computer-Aided Assessment and Control Localized Damage*, Udine, Italy., 1994.

[31] M. H. Sadd, Q. Dai, V. Parameswaran and A. Shukla, "Simulation of asphalt materials using finite element micromechanical model with damage mechanics," *Transportation Research Record,* pp. 86-95, 2004.

[32] H. H. Chen, K. M. Marshek and L. Chhote, "Effects of Truck Tire Contact Pressure Distribution on the Design of Flexible Pavements: A Three- Dimensional Finite Element Approach," *Transportation Research Record,* no. 1095, pp. 72-78, 1990.

[33] "ABAQUS: Version 6.9," Providence, RI, 2009.

[34] S. Helwany, D. John and J. Leidy, "Finite-Element Analysis of Flexible Pavements," *Transportation Engineering,* vol. 124, no. 5, pp. 491-498, 1998.

[35] Q. Dai, M. H. Sadd and Z. You, "A micromechanical finite element model for viscoelastic creep and viscoelastic damage behavior of asphalt mixture," *Int J Numeric Anal Meth Geomech,* p. 1135–1158, 2006.

[36] R. K. Abu Al-Rub R.K., T. You, E. Masad E. and D. Little, "Mesomechanical modeling of the thermo-viscoelastic, thermo-viscoplastic, and thermo-viscodamage response of asphalt concrete," *Int. J. Eng. Sci,* vol. 28, 2011.

[37] M. K. Darab, R. Abu Al-Rub, E. Masad and Huan, "A thermo-viscoelastic-viscoplastic-viscodamage constitutive model for asphalt materials," *Int. J. Solids Struct,* vol. 48, pp. 191-207, 2011.

[38] J. Hau, "Finite element modeling and analysis of accelerated pavement testing devices and phenomenon," Ph.D. Dissertation, Purdue University, 2000.

[39] J. E. S. Lutif, F. V. Souza, Y. Kim, J. B. Soares and D. H. Allen, "Noninvasive Measurement of Permanent Strain Field Resulting from Rutting in Asphalt Concrete," *Transportation Research Board,* no. 2181, pp. 28-35, 2009.

[40] E. Aigner, R. Lackner and C. Pichler, "Multiscale Prediction of Viscoelastic Properties of Asphalt Concrete," *Materials in Civil Engineering,* vol. 21, no. 12, 2009.

[41] S. Ghosh, K. Lee and P. Raghavan, "A Multi-level Computational Model for Multiscale Damage Analysis in Composite and Porous Materials," *International Journal of Solids and Structures,* vol. 38, pp. 2335-2385, 2001.

[42] R. M. Haj-Ali and A. H. Muliana, "A Multi-scale Constitutive Formulation for the Nonlinear Viscoelastic Analysis of Laminated Composite Materials and Structures," *International Journal of Solids and Structures,* vol. 41, pp. 3461-3490, 2004.

[43] L. Wang, J. D. Frost and J. S. Lai, "Noninvasive Measurement of Permanent Strain Field Resulting from Rutting in Asphalt Concrete," *Transportation Research Board,* no. 1687, p. 85–94, 1999.

[44] A. Coenen, M. Kutay and H. Bahia, "Aggregate Structure Characterization of Asphalt Mixtures Using 2-Dimensional Image Analysis," *International Journal of Road Materials and Pavement Design,* 2011.

[45] "MATLAB: Version 7.12," The MathWorks Inc, 2011.

[46] E. Masad, V. K. Jandhyala, N. Dasgupta, N. Somadevan and N. Shashidhar, "Characterization of Air Void Distribution in Asphalt Mixes using X-ray Computed Tomography," *JOURNAL OF MATERIALS IN CIVIL ENGINEERING,* vol. 14, no. 2, pp. 122-129, 2002.

[47] L. Wang, H. Paul, T. Harman and J. Angelo, "Characterization of Aggregates and Asphalt Concrete using X-ray Tomography," *AAPT,* vol. 73, pp. 467-500, 2004.

[48] L. Tashman, E. Masad, B. Peterson and H. Saleh, "Internal Structure Analysis of Asphalt Mixes to Improve the Simulation of Superpave Gyratory Compaction to Field Conditions," *Journal of the Association of Asphalt Paving Technologists,* vol. 70, pp. 605-645, 2001.

[49] W. G. Buttlar and Z. You, "Discrete Element Modeling of Asphalt Concrete," *Transportation Research Record,* no. 1757, pp. 111-118, 2000.